

Authors' response

Based on the reviewer comments the manuscript has been largely rewritten. In the following, we give a short summary of the changes followed by the response to the reviewers and a difference file created by *latexdiff* showing all changes.

The title has been changed to “*Development of a custom OMI NO₂ data product for evaluating biases in a regional chemistry transport model*” to account for the stronger focus on biases in the satellite product.

The affiliation of first and second author has been extended.

The introduction (Sect. 1) has been rewritten and shortened based on the suggestions by the reviewer.

Some small changes have been applied to the background section (Sect. 2).

In the method section (Sect. 3), the two data processing subsections for HKOMI and CMAQ were merged and moved to the end of the section. A new subsection (Evaluation study) has been added which describes briefly the comparison done in our study.

The sections “results and discussions” and “discussions and conclusions” have been split in three sections: “results”, “discussions” and “conclusions”. This allows a more general discussion of the results and removes some repetitions. The discussions section has been extended to include much more discussions and references. The conclusions have been reduced moving large parts to the new discussions section.

A new OMI datasets has been added which computes AMFs with OMNO₂ scattering weights and CMAQ profiles (OMNO₂-SW). The influence of the ancillary parameters is now estimated by the differences (NMB and CV) between the six OMI datasets being more consistent. Examples are only used for further illustration. These changes allow for better comparison with other custom products.

We removed table 1 and added a new table which shows NMB and CV between the six OMI datasets. The appendix has been moved into a new table. Figures 6 and 8 have been removed to the supplement.

Interactive comment on “Evaluation of a regional chemistry transport model using a newly developed regional OMI NO₂ retrieval” by G. Kuhlmann et al.

G. Kuhlmann et al.

gerrit.kuhlmann@gmail.com

Received and published: 19 April 2015

We like to thank reviewer 1 for his or her detailed feedback. As suggested we did a major revision of the manuscript which is attached to this reply.

The title has been changed to “Development of a custom OMI NO₂ data product for evaluating biases in a regional chemistry transport model”. Furthermore, first and second authors’ affiliations have been extended. The abstract was also rewritten to account for the changes in the manuscript. The introduction (Sect. 1) has been rewritten and shortened based on the suggestions. Some small changes have been applied to

C13018

the background section (Sect. 2).

In the method section (Sect. 3), the two data processing subsections for HKOMI and CMAQ were merged and moved to the end of the section. A new subsection (Evaluation study) has been added which describes briefly the comparison done in our study.

The sections “results and discussions” and “discussions and conclusions” have been split in three sections: “results”, “discussions” and “conclusions”. This allows a more general discussion of the results and removes some repetitions. The discussions section has been extended to include much more discussions and references. The conclusions have been reduced moving large parts to the new discussions section.

A further OMI datasets has been added which computes AMFs with OMNO₂ scattering weights and CMAQ profiles (OMNO₂-SW). The influence of the ancillary parameters is now estimated by the differences (NMB and CV) between the six OMI datasets being more consistent. Examples are only used for further illustration. These changes allow for better comparison with other custom products. We removed table 1 and added a new table which shows NMB and CV between the six OMI datasets. The appendix has been moved into a new table. Figures 6 and 8 have been removed to the supplement.

Reply to general comments:

To 1) The naming convention and acronyms have been revised following the suggestion by reviewer 1. Wrong spelling and grammar have been corrected.

To 2) The paper has been shortened from 52 to 50 pages. This was achieved by removing some figures and tables to the supplement as well as by removing repetitions.

To 3) In the extended discussion section, we provide a more detailed comparison with other custom retrievals and evaluation studies.

C13019

Reply to specific comments:

To 1) As suggested, a new dataset has been included which computes AMFs using CMAQ NO₂ profiles and scattering weights (OMNO₂-SW). Furthermore, we agree that including DOMINO would be beneficial for this study. However, including the DOMINO data product would widen the scope of our study too much for one paper and will be left for future studies.

To 2) We provide now a brief explanation of averaging kernels and their influence on NO₂ VCDs in the introduction and in the discussions. The expected real NO₂ profile is discussed in Section 5.1.

To 3) We removed the discussion of old OMI NO₂ standard retrievals from the introduction and focus instead on the latest version.

To 4) We agree that it would be more plausible to use the CMAQ model grid instead of a 0.01°×0.01° grid. However, the gridding algorithm currently only supports longitude-latitude grids. This is explained in the paper now. We also added that 0.01°×0.01° is about 1×1 km² in the PRD region.

Reply to technical corrections:

Product names and OMI-related terminology have been corrected and are more consistent now. We adopted the suggested name for our custom product: Hong Kong OMI NO₂ (HKOMI) product. Furthermore, we are using the term standard and custom products now. The term “datasets” is used to describe the compiled NO₂ observations or simulations from OMI or CMAQ, respectively. We are also using level-2 for swath-level and level-3 for gridded data and are avoiding the potential misleading term global product for level-3 products. The title has been changed to

C13020

account for the changed name. Grammatical errors have been corrected.

Please also note the supplement to this comment:

<http://www.atmos-chem-phys-discuss.net/14/C13018/2015/acpd-14-C13018-2015-supplement.pdf>

Interactive comment on Atmos. Chem. Phys. Discuss., 14, 31039, 2014.

C13021

Interactive comment on “Evaluation of a regional chemistry transport model using a newly developed regional OMI NO₂ retrieval” by G. Kuhlmann et al.

G. Kuhlmann et al.

gerrit.kuhlmann@gmail.com

Received and published: 19 April 2015

Response to Reviewer 3

We like to thank reviewer 3 for his or her feedback. The manuscript has undergone a major revision based your and reviewer 1's comments. The updated manuscript is attached as supplement to this reply.

C13022

1 Reply to minor points:

To 1) We agree that improved CTM performance, mainly by updating our emission inventory, should greatly improve the HKOMI retrieval. This has been included in the updated manuscript (Section 5.3 and 5.4).

To 2) We did not test different CRFs filter thresholds. Since CRFs in the PRD region are frequently high, a larger threshold is required to obtain a sufficient number of data (see also Chan et al., AMT, 2012). The CRF filter threshold can influence mean NO₂ VCDs, because NO₂ concentrations can differ between clear and overcast conditions. However, the CRF filter does not change the major findings of our study, because ground measurements and CMAQ fields were temporally collocated with the OMI datasets.

To 3) The introduction has been rewritten and the sentence was removed.

Please also note the supplement to this comment:

<http://www.atmos-chem-phys-discuss.net/14/C13022/2015/acpd-14-C13022-2015-supplement.pdf>

Interactive comment on Atmos. Chem. Phys. Discuss., 14, 31039, 2014.

C13023

Evaluation Development of a custom OMI NO₂ data product for evaluating biases in a regional chemistry transport model using a newly developed regional OMI retrieval

G. Kuhlmann^{1,2}, Y. F. Lam^{1,3}, H. M. Cheung¹, A. Hartl¹, J. C. H. Fung⁴,
P. W. Chan⁵, and M. O. Wenig⁶

¹School of Energy and Environment, City University of Hong Kong, Hong Kong, China

²Empa, Swiss Federal Laboratories for Materials Science and Technology, Dübendorf, Switzerland

³Guy Carpenter Asia-Pacific Climate Impact Centre, School of Energy and Environment, City University of Hong Kong, Hong Kong, China

⁴Department of Mathematics, The Hong Kong University of Science & Technology, Hong Kong, China

⁵Hong Kong Observatory, Hong Kong, China

⁶Meteorologisches Institut, Ludwig-Maximilians-Universität, Munich, Germany

Correspondence to: G. Kuhlmann (gerrit.kuhlmann@my.cityu.edu.hk) and
Y. F. Lam (yunflam@cityu.edu.hk)

Abstract. In this paper, we ~~evaluate a high-resolution chemistry transport model (CTM) (3 km × 3 km spatial resolution) with the new Hong Kong (HK) present the custom Hong Kong~~ NO₂ retrieval ~~developed (HKOMI) for the Ozone Monitoring Instrument (OMI) on-board on board the Aura satellite~~. ~~The three-dimensional atmospheric chemistry which was used to evaluate a high-resolution~~
5 ~~chemistry transport model (CTM) (3 km × 3 km spatial resolution). The atmospheric chemistry transport~~ was modelled in the Pearl River Delta (PRD) region in southern China by the Models-3 Community Multiscale Air Quality (CMAQ) modelling system from October 2006 to January 2007. In the ~~HK-HKOMI~~ NO₂ retrieval, tropospheric air mass factors (AMF) were recalculated using high-resolution ancillary parameters of surface reflectance, ~~a priori~~ NO₂ ~~profile shapes~~ and aerosol
10 profiles of which the latter two were taken from the CMAQ simulation. We ~~also tested tested the influence of the ancillary parameters on the data product using~~ four different aerosol parametrizations. Ground level measurements by the PRD Regional Air Quality Monitoring (RAQM) network were used as additional independent measurements.

The ~~HK retrieval increases the HKOMI retrieval increases estimated tropospheric~~ NO₂ vertical column densities (VCD) by $(+31 \pm 38) \%$, when compared to NASA's standard product (~~SP2OMNO2-SP~~), and ~~reduces the improves the normalised~~ mean bias (~~MBNMB~~) between satellite and ground ~~measurements observations~~ by 26 percentage points from -41 to -15% . The ~~individual influences of the parameters are~~ $(+11.4 \pm 13.4) \%$ for NO₂ profiles, $(+11.0 \pm 20.9) \%$ for surface reflectance and $(+6.0 \pm 8.4) \%$ for the best aerosol parametrisation. The correlation coefficient r is

20 low ~~for both satellite datasets~~ between ground and satellite observations ($r = 0.35$) ~~due to the high~~
~~spatial variability of concentrations.~~ The low r and the remaining NMB can be explained by the
low model performance and the expected differences when comparing point measurements with
area-averaged satellite observations.

The correlation between CMAQ and the RAQM network is low ($r \approx 0.3$) and the model under-
25 estimates the NO_2 concentrations in the north-western model domain (Foshan and Guangzhou).
We compared the CMAQ NO_2 time series of the two main plumes with our ~~regional best~~ OMI
 NO_2 ~~product dataset~~ (HKOMI-4). The model overestimates the NO_2 VCDs by about 15 % in Hong
Kong and Shenzhen, while the correlation coefficient is satisfactory ($r = 0.56$). In Foshan and
Guangzhou, the correlation is low ($r = 0.37$) and the model underestimates the VCDs strongly
30 ~~(MB = -40 NMB = -40 %)~~. In addition, we estimated that the OMI VCDs are also underestimated
by about 10 to 20 % in Foshan and Guangzhou because of the influence of the model parameters on
the ~~AMF~~ AMFs.

In this study, we demonstrate that the ~~HK OMI~~ HKOMI NO_2 retrieval reduces the bias of the
satellite ~~measurements and thus observations and how~~ the dataset can be used to study the magnitude
35 of NO_2 concentrations in a regional model at high spatial resolution of 3×3 km². The low bias
~~can be achieved if AMFs are recalculated with more accurate~~ was achieved with recalculated AMFs
using updated surface reflectance, aerosol profiles and NO_2 profiles; ~~only profiles have been replaced~~
~~in earlier studies~~. Since unbiased concentrations are important, for example, in air pollution studies,
the results of this paper can be very helpful in future model evaluation studies.

40 1 Introduction

Nitrogen oxides ($\text{NO}_x = \text{NO} + \text{NO}_2$) play an important role in atmospheric chemistry.
~~They have a vital role~~ As precursors of ozone and aerosols, they are vital in the forma-
tion of photochemical smog (Haagen-Smit, 1952) and ~~can damage crops and buildings as~~
~~a component of~~ acid rain (Driscoll et al., 2001). In ~~an urban environment~~ the troposphere,
45 NO_2 concentrations have a high spatial and temporal variability due to ~~its short tropospheric~~
~~life time~~ their short lifetime and the variety of sources and sinks. ~~The spatial and~~
~~temporal distribution can be~~ This spatiotemporal variability has been studied with chem-
istry transport models (CTM), air quality monitoring networks and satellite instruments
(e.g. Beirle et al., 2003; Huijnen et al., 2010; Han et al., 2011; Chan et al., 2012; Han et al., 2015; Mueller et al., 2015).

50 The first satellite instrument able to detect tropospheric NO_2 was the Global Ozone Monitoring
Experiment (GOME) which was launched on board the second European Remote Sensing satellite
(ERS-2) in 1995 (Burrows et al., 1999). Successor instruments to GOME (GOME-2) are payload on
the MetOp satellites used for operational meteorology (Callies et al., 2000). In 2006, the Scanning
Imaging Absorption Spectrometer for Atmospheric Cartography (~~SCIAMACHY~~ SCIAMACHY) was

55 launched on board ~~ENVISAT (ENVIronmental SATellite~~ the ENVIronmental SATellite (ENVISAT)
(Bovensmann et al., 1999) and in 2004, the Ozone Monitoring Instrument (OMI) was launched on
board the ~~EOS (Earth Observation System) Aura~~ Aura satellite (Levelt et al., 2006). Since the launch
of GOME, the spatial resolution of the instruments increased rapidly. While GOME had a smallest
ground pixel size of 40 km × 320 km, that was suitable for coarse global analyses, OMI has a smallest
60 ground pixel size of 13 km × 24 km. The higher spatial resolution makes OMI ~~feasible~~ applicable
for the study of ~~trace gases~~ NO₂ in large metropolitan areas.

The ~~two~~ OMI NO₂ standard products are the NASA standard product (SPOMNO2, Version 2.1)
(Bucsela et al., 2006, 2013) and the ~~the Dutch OMI Derivation of OMI tropospheric~~ NO₂ prod-
uct (DOMINO) (~~Boersma et al., 2007, 2011~~) ~~which are both available in their second version (SP2~~
65 ~~and DOMINO-2)~~. In this paper, we use the term “global” products for this two products because
they provide global coverage. In contrast, “regional” products provide regional coverage. Examples
~~of regional OMI, Version 2.0 (Boersma et al., 2007, 2011)~~. The NO₂ products are the Empa
product for Europe (Boersma et al., 2007; Zhou et al., 2009; Zhou et al., 2010) and the Berkeley
High-Resolution (BEHR) product for North America (Russell et al., 2011). It should be noted that
70 in literature the term “global” is often used as a synonym for “level 3” data that has had orbit-level
data (“level 2”) combined onto a global grid. This terminology can be misleading, because “level
3” data can also be provided on a local or regional grid. For example, the grid can be the domain
of a regional CTM. A second difference between regional and global products is the spatiotemporal
resolution of the ancillary parameters used in their retrieval algorithms. Ancillary parameters are
75 ~~information about retrieval algorithms use ancillary parameters, such as~~ surface reflectance, a priori
NO₂ profile shapes, aerosols and clouds which are used profiles, and aerosol and cloud information,
to calculate air mass factors (AMF) ~~which~~. The AMFs convert the retrieved NO₂ slant column
densities (SCD) to vertical column densities (VCD). In the ~~first version of SP and DOMINO, the~~
~~ancillary parameters were mainly monthly or annual averages with spatial resolutions between~~
80 ~~50 and 300~~ standard products, a priori NO₂ profiles are taken from global CTMs with a spatial
resolution of 2° ×. In contrast, regional products use ancillary parameters with a higher spatial and
temporal resolution. For example, Zhou et al. (2010) used surface reflectance with 12.5° (OMNO2)
and 2° × spatial resolution to improve the retrieval in Europe and Russell et al. (2011) replaced the
profile shapes from a global CTM with profiles from a regional CTM with a 3° (DOMINO). Surface
85 reflectances are taken from an OMI climatology with a spatial resolution of 40.5° ×. Thus, we use the
terms “regional” and “global” for products which use ancillary parameters which have a spatial and
temporal resolution typical for a regional or global CTM, respectively 0.5° (Kleipool et al., 2008).

Russell et al. (2011) compared the BEHR product with the first version of the DOMINO and
the NASA product and showed that the retrieved Since NO₂ VCDs are strongly impacted
90 by terrain pressure (±20), surface reflectance (±40) and the profile shape (−75 ± 10%).
Lin et al. (2014) showed that different ancillary parameters can have a strong profile and surface

reflectance have a large impact on the NO₂ VCDs. Furthermore, the global products have been compared with regional CTMs. Since the OMI VCDs depend on the VCD, the standard products are not directly suitable to study VCDs on a scale below the resolution of these ancillary parameters.

95 However, when more accurate NO₂ profile shapes, the global profile shapes can and should be replaced with the profiles of the regional model (Eskes and Boersma, 2003; Boersma et al., 2005). The global OMI profiles are available, for example in model evaluation studies, the VCDs can be corrected using scattering weights (SW) or averaging kernels (AK). The correction removes the dependency on the a priori profile and can be applied either to the OMI NO₂ products

100 provide data for this update. Several studies evaluated regional CTMs with the global products using updated profiles. Herron-Thorpe et al. (2010) validated the regional VCDs or the model profiles (for details see Eskes and Boersma, 2003; Boersma et al., 2005). SW and AK are closely related to vertically resolved AMFs and are provided with the standard products. AKs have been applied, for instance, by Herron-Thorpe et al. (2010), who validated the regional-scale air quality model

105 AIRPACT-3 (12 km × 12 km spatial resolution) over the Pacific Northwest with the first versions of DOMINO and the NASA product. Their simulations correlate well with the monthly averaged satellite measurements for cloud-free data ($r = 0.75$) as long as no wildfires are present in the model domain. Han et al. (2011) compared CMAQ simulation (30 km × 30) with the first DOMINO version over the Korean peninsula and found that simulated VCDs are about 50 larger than satellite

110 measurements. Zyrihidou et al. (2013), and Zyrihidou et al. (2013), who evaluated the Comprehensive Air Quality Model (CAMx) (10 km × 10 km) over Southeastern Europe with the second DOMINO version. They found good agreement between model and OMI VCDs ($r = 0.6$), but the model overestimated VCDs over urban areas. Applying AKs has a large influence on the magnitude of tropospheric NO₂ VCDs (Herron-Thorpe et al., 2010).

115 In SP2 and DOMINO-2, the spatial and temporal resolutions of several ancillary parameters have been increased. For example, the products are using the OMI reflectance climatology (0.5 spatial resolution) and standard products, AKs and SWs depend on the OMI surface reflectance climatology. The spatial resolution of this climatology is coarse compared to the OMI ground pixel size. Therefore, customised NO₂ profile shapes are corrected using a products

120 have been developed which recalculate AKs, and thus AMFs, using high-resolution topography (3). Nevertheless, the global products still depend on a global CTM which have limited spatial resolution. As a consequence, the global products can be biased, if surface reflectance products (Zhou et al., 2010; Russell et al., 2011; McLinden et al., 2014). Furthermore, AKs and SWs are affected by aerosols directly due to additional scattering and absorption (Leitão et al., 2010) as

125 well as indirectly due to their impact on the retrieval of surface reflectance and cloud properties (Boersma et al., 2011; Lin et al., 2014). Since the ancillary parameters have a large impact on the magnitude of the retrieved NO₂ VCDs are studied on regional scale, it is important to consider

their influence, for example, in air pollution studies where unbiased pollutant concentrations are important.

130 ~~In this study, we evaluate a regional CTM (3 km × 3 km spatial resolution) with a regional~~ For this paper, we developed a customized OMI NO₂ retrieval ~~. For this purpose, we simulated three-dimensional atmospheric chemistry with the Models-3 Community Multiscale Air Quality (CMAQ) modelling system (Byun and Schere, 2006) in the and applied it to the Pearl River Delta (PRD) region in southern China from October.~~ The Hong Kong OMI (HKOMI) retrieval
135 recalculates tropospheric AMFs and uses them with OMNO2 SCDs to calculate VCDs. The HKOMI product was used to evaluate the Models-3 Community Multiscale Air Quality (CMAQ) modelling system (3 km × 3 km spatial resolution) (Byun and Schere, 2006). The study period is October 2006 to January to January 2007. Furthermore, we developed a new regional retrieval for the PRD region. In the Hong Kong (HK) retrieval, we recalculated tropospheric AMFs
140 using high-resolution ancillary parameters which were taken mainly from the CMAQ simulation. Thus, the retrieval does not depend on other models. Cloud height and fraction were taken from the OMI cloud product (Acarreta et al., 2004) and surface reflectance was calculated from the MODIS (Moderate-resolution Imaging Spectroradiometer) black-sky albedo (BSA) product (Wanner et al., 1997; Lucht et al., 2000). We tested different aerosol parametrizations for our new
145 product. Aerosol extinction and absorption coefficients were computed from the model output. As additional and independent observations, ground level measurements were used from 16 Three automatic weather stations and sixteen ground level stations of the PRD Regional Air Quality Monitoring (RAQM) network ~~. To the best of our knowledge, this is the first study in which a regional OMI were used to validate model and retrieval. The objective is to estimate the influence of the ancillary parameters on the evaluation and to demonstrate some possibilities and limitations for using satellite-based NO₂ product is compared with a regional CTM observations.~~

This paper is organised as follows: OMI and the retrieval of tropospheric NO₂ including the AMF calculations using the SCIATRAN radiative transfer model are described ~~briefly~~ in Sect. 2. The RAQM network, the CMAQ model run ~~, the HK and the HKOMI~~ NO₂ retrieval are described
155 in Sect. 3. The results are presented in Sect. 4 and discussed in Sect. 4.5. Finally, Sect. 6 ~~contains further discussions and~~ concludes this paper.

2 Background

2.1 Ozone Monitoring Instrument (OMI)

OMI is a nadir-viewing imaging spectrometer measuring Earth's reflectance spectra in the near-ultraviolet and visible wavelength range with two ~~CCD~~ (charge-coupled device (CCD)) arrays. It was
160 launched aboard NASA's EOS Aura satellite on 15 July 2004 (Levelt et al., 2006). The instrument provides near daily global coverage at an overpass time of 13:45 ± 15 ~~min~~ minutes ~~LT~~ Local time (LT).

Earth reflectance spectra are measured during the sunlit part of about 14.5 sun-synchronous orbits per day. Trace gases, such as ozone (O₃), sulfur dioxide (SO₂) and nitrogen dioxide (NO₂), are retrieved from the reflectance spectra as well as cloud and aerosol properties.

The measurement principle is an along-track (push-broom) scanner with a swath width of 2600 km which is divided ~~in into~~ 60 pixels. The ground pixel size varies between 13 km × 24 km at nadir and 40 km × 160 km at the swath edge (Levelt et al., 2006). ~~Since June 2007, OMI is affected by a row anomaly which reduces the number of valid measurements (see http://www.knmi.nl/omi/research/product/rowanomaly-background.php for details). The spatial sensitivity within a ground pixel is nearly constant in across-track direction but decreases in along-track direction.~~

2.2 ~~Retrieval~~ Standard retrieval of tropospheric NO₂ column densities

The ~~standard product (SP2) (Bucsela et al., 2006, 2013)~~ OMNO2 product is the basis for the ~~HK~~ HKOMI retrieval. Therefore, we give a brief introduction to their algorithm. The ~~SP2-OMNO2~~ retrieval algorithm has three major steps:

1. The total slant column densities S are obtained from the reflectance spectra using the differential optical absorption spectroscopy (DOAS) technique (Platt and Stutz, 2008).
2. The stratospheric slant column densities S_{strat} are subtracted from the total column S using a stratosphere–troposphere separation (STS) algorithm (Bucsela et al., 2013).
- 180 3. The tropospheric slant column densities S_{trop} are converted to vertical column density V_{trop} using a tropospheric air mass factors (AMF) A_{trop} (Palmer et al., 2001).

The AMF is defined as the ratio of slant and vertical column density (Solomon et al., 1987). Thus the tropospheric column density V_{trop} is calculated by

$$V_{\text{trop}} = \frac{S - S_{\text{strat}}}{A_{\text{trop}}} = \frac{S_{\text{trop}}}{A_{\text{trop}}}. \quad (1)$$

The tropospheric AMF depends on parameters such as sun position, ~~satellite position~~ instrument viewing direction, surface reflectance, atmospheric scattering properties due to air molecules, aerosols and clouds, and the a priori NO₂ profile ~~shape~~. It is related to the vertical sensitivity of the satellite instrument and can be computed for N vertical layers by

$$A_{\text{trop}} = \frac{\sum_{k=1}^N \alpha_k m_k V_k}{\sum_{k=1}^N V_k} \quad (2)$$

with:

- α_k : an empirical temperature correction coefficient accounting for the temperature dependency of the NO₂ absorption cross section,
- 195 – m_k : the differential or box air mass factor which describes the instrument sensitivity for layer k ,

- V_k : the partial NO₂ VCD of layer k .

The products $\alpha_k m_k$ are the scattering weights provided with the standard product. The correction coefficient α_k can be computed by the empirical formula

$$200 \quad \alpha_k = 1 - 0.003 \text{K}^{-1} (T_k - T_{\text{ref}}) \quad (3)$$

where T_k is the temperature in layer k and T_{ref} is reference temperature of the NO₂ absorption cross section ($T_{\text{ref}} = 220 \text{K}$) (Bucsela et al., 2013).

The box air mass factors m_k can be computed with a radiative transfer model. The SP2-OMNO2 algorithm uses the TOMRAD radiative transfer model (Dave, 1965). The AMF formulation used in SP2-OMNO2 is based on a AMF formulation by Palmer et al. (2001). In partly cloudy scenes, SP2-OMNO2 computes the box AMFs using the independent pixel approximation (IPA). The approximation calculates AMFs as weighted sums of a cloudy m_k^{cloudy} and a clear m_k^{clear} component:

$$210 \quad m_k = w \cdot m_k^{\text{cloudy}} + (1 - w) \cdot m_k^{\text{clear}}, \quad (4)$$

where w is the aerosol/cloud radiance fraction (CRF), that is the fraction of measured radiation that results from clouds and aerosols (Acarreta et al., 2004).

~~The products $\alpha_k m_k$ are called scattering weights. They can be used to recalculate the AMF with different profile shapes which could be taken from a regional CTM.~~

215 ~~In~~ SP2-OMNO2, the partial VCD V_k are taken from the Global Modeling Initiative (GMI) CTM (Duncan et al., 2007; Strahan et al., 2007) which combines stratospheric chemistry described by Douglass et al. (2004) and tropospheric O₃-NO_x-hydrocarbon chemistry from the GEOS-Chem model (Bey et al., 2001). It should be noted that, for an optical thin absorber, only the relative shape of the profile $n_k = V_k/V_{\text{trop}}$ is required for the AMF calculation.

220 Bucsela et al. (2013) estimated tropospheric NO₂ VCD uncertainties to be $1 \times 10^{15} \text{cm}^{-2}$ for clear skies and up to $3 \times 10^{15} \text{cm}^{-2}$ for large cloud radiance fractions. In polluted regions, the main uncertainties are ~~in~~ the DOAS fit (10 % relative error) and ~~in~~ the tropospheric AMFs (20–80 %).

2.3 SCIATRAN radiative transfer model

225 SCIATRAN is a one-dimensional RTM which can be used for the calculation of box AMFs (Rozanov et al., 2005). The model is designed as a forward model for the retrieval of atmospheric constituents from measurements of scattered light by satellite, ground or airborne instruments. The wavelength range goes from 175 to 2380 nm which includes the ultra violet, visible and near ~~infra-red~~ infra-red part of the spectrum.

230 SCIATRAN solves the integro-differential radiative transfer equation using the discrete-ordinates method (DOM) in the plane-parallel or pseudo-spherical mode to calculate box AMF profiles. Box AMFs m_k are derived from weighting functions which describe the sensitivity of the reflectance

spectrum R to a perturbation of a model parameter Δn in layer z_k . In SCIATRAN, weighting functions are computed by a quasi-analytic approach (Rozanov et al., 1998). If Δn is a perturbation of the NO_2 number density n_k , the box AMF m_k is the negative weighting function (Rozanov and
235 Rozanov, 2010).

3 Methodology

In this section, we describe the RAQM network, the ~~regional CTM run and the HK CMAQ CTM~~
~~and the HKOMI~~ retrieval. Our study period is from October 2006 to January 2007. ~~This period was~~
~~2007 which has been~~ chosen because cloud fractions in the PRD region are lowest in this season and
240 OMI measurements in later years are affected by ~~a row anomaly which reduces the number of valid~~
~~measurements. Details about the row anomaly can be found on the aforementioned row anomaly.~~

3.1 Ground ~~network~~ networks

3.1.1 Meteorological observations

Meteorological observations were used for the evaluation of the simulated meteorological fields
245 which were used to drive the CTM. The data were measured by three automatic weather stations
in Hong Kong. The stations are located at the Hong Kong Observatory (HKO) headquarters, ~~at the~~
Hong Kong International Airport (HKIA) ~~near Tung Chung~~ and on Waglan Island (WGL). ~~The~~
~~locations of the stations are shown by square markers in (see Fig. 1. The Hong Kong Observatory).~~
HKO is in the city centre of Kowloon and surrounded by high buildings. ~~The airport HKIA~~ is located
250 on an artificial island near Tung Chung to the north of mountainous Lantau Island. Waglan Island
is a small island located to the east of Hong Kong Island. The island is too small to be resolved by
the model grid. The WGL station is located 56 m above sea level and used as background station
by the Hong Kong Observatory. The used meteorological parameters are hourly measurements of
temperature (T), humidity (q), sea surface pressure (p) and wind (v). Temperature and humidity ~~are~~
255 have been measured at 2 m above ground level (a.g.l.).

3.1.2 Pearl River Delta Regional Air Quality Monitoring Network

Ground-level NO_2 mixing ratios were provided by the RAQM network. The network was established
by the governments of the Guangdong province and Hong Kong to monitor the air quality in the PRD
region and has been in operation since 30 November 2005. It consists of sixteen automatic air quality
260 monitoring stations (see Fig. 1, round markers). The network measures ~~hourly~~- NO_2 , SO_2 , O_3 and
 PM_{10} hourly. The monitoring network was used to validate the NO_2 mixing ratios of the OMI NO_2
products and the CMAQ simulation. In the network, NO_2 ~~was is~~ measured by chemiluminescence
and DOAS technique with an accuracy and precision of about 10 % (GDEMC and HKEPD, 2006).

3.2 CMAQ model simulation

265 3.2.1 Model run

~~Three dimensional atmospheric~~ Atmospheric chemistry was simulated ~~in the PRD region for the study period. The simulations were performed~~ with the CMAQ modelling system version 4.7.1 (Byun and Schere, 2006).

Three model domains were defined using a Lambert conformal conic projection (Fig. 1). The coarse domain (D1) covers East Asia with a spatial resolution of $27\text{ km} \times 27\text{ km}$. The nested domains have grid resolutions of $9\text{ km} \times 9\text{ km}$ (D2) and $3\text{ km} \times 3\text{ km}$ (D3), ~~receptively~~ respectively.

Meteorological fields were provided by the Weather Research and Forecasting (WRF) modelling system (Skamarock et al., 2008) driven by NCEP Final Analysis (FNL) data (NCEP et. al., 1997). Horizontal advection was modelled ~~by~~ with the mass-conserving YAMO scheme (Yamartino, 1993). The default vertical advection scheme was replaced ~~with the WRF omega calculation with the piecewise parabolic method. The new scheme is the default scheme~~ by the new advection scheme implemented in CMAQ version 5 ~~and is assumed to provide better vertical profiles. Accurate vertical profiles are important for satellite measurements of air pollutants.~~ 5.

The gas-phase chemistry was modelled ~~by~~ with the Euler backward iterative solver optimized for the Carbon Bond-05 mechanism with chlorine (Yarwood et al., 2005). Aerosol chemistry was modelled ~~by~~ with the fifth-generation CMAQ aerosol model (aero5) ~~and while~~ the impact of clouds on deposition, mixing, photolysis, and aqueous chemistry was ~~described by the ACM set by the Asymmetrical Convective Model (ACM)~~ cloud processor (Pleim and Chang, 1992). Three-dimensional extinction coefficients were computed by the empirical IMPROVE formula (Malm et al., 1994).

The emission inventory used in this simulation was compiled by Du (2008). The inventory combines monthly anthropogenic emission from INTEX-B (Zhang et al., 2009) with biogenic emissions from GEIA (Global Emissions Inventory Activity, Guenther et al., 1995), and biomass burning and ship emissions from TRACE-P (Streets et al., 2003). The INTEX-B emissions were updated with regional emissions for Hong Kong ~~provide~~ provided by the Hong Kong Environmental Protection Department (Du, 2008). ~~The low-resolution emissions were spatially allocated to each grid cell based on geographic and socio-economic information as well as updated road network and land cover data. Furthermore, weekly and daily cycles were included to the emission inventory (Du, 2008).~~

3.2.1 Data processing

295 ~~Model outputs are~~ Model outputs used were hourly ground level values and three-dimensional fields of NO_2 mixing ratios, aerosols and meteorological parameters averaged from 13:00 to 15:00 LT (OMI overpass time).

In addition, at each ground ~~stations~~station, time series of hourly meteorological parameters and NO₂ mixing ratios were extracted from the model output. The surface pressure in the model was converted to sea level pressure using the simulated temperature. The wind vector in the model was taken at the height of the measurement stations to account for the elevation of the stations above averaged surface height.

~~Since OMI has a lower spatial resolution than CMAQ, the satellite instrument cannot resolve high-frequency features in the simulated distribution. Therefore, the two datasets were made comparable by averaging the CMAQ data for each OMI ground pixel in an orbit. The pixel boundaries were provided by the overlapping ground pixel product. Within the boundaries, each grid point was weighted based on the instrument's spatial sensitivity (Dobber et al., 2006; Kurosu and Celarier, 2010). Since the set of averaged data is not conveniently visualisable, the CMAQ data were projected back onto a $0.01^\circ \times 0.01^\circ$ longitude-latitude grid using a recently developed gridding algorithm (Kuhlmann et al., 2014). The gridding algorithm is available at: . In this step, missing OMI pixels were also removed from the CMAQ data. Using this approach, the distributions of OMI and CMAQ are directly comparable.~~

3.3 The Hong Kong OMI (HKOMI) NO₂ retrieval

3.4 ~~The Hong Kong (HK) OMI retrieval~~

~~For the HK~~For the HKOMI NO₂ retrieval, we recalculated tropospheric AMFs ~~by~~with Eq. (2) with new ancillary parameters. The new AMFs were used to compute the tropospheric VCDs ~~by~~with Eq. (1).

For the AMF calculation, a set of ancillary parameters was ~~put together~~compiled for each OMI ground pixel. The parameters were taken mainly from the WRF/CMAQ simulation. Thus, the retrieval does not depend on any other CTM model which makes the model evaluation easier. The ~~ancillary~~ parameters are surface elevations, temperature, pressure and NO₂ profiles, ~~and as well as~~ aerosol extinction coefficients. ~~The model domain (D3, Fig. 1) has a spatial resolution of $3\text{ km} \times 3$. The WRF/CMAQ data were temporally averaged to the OMI overpass time.~~ Further ancillary parameters are cloud height and ~~aerosol/cloud radiance fraction (CRF)~~CRF, which were taken from the OMI O₂-O₂ cloud product (Acarreta et al., 2004), and surface reflectance, which was taken from the MODIS MCD43C2 ~~black-sky albedo (BSA)~~ product (Wanner et al., 1997; Lucht et al., 2000). ~~Table ?? compares the updated parameters with the ancillary parameters used in SP2.~~

All ancillary parameters were projected to a $0.01^\circ \times 0.01^\circ$ ~~(about $1\text{ km} \times 1\text{ km}$)~~ longitude-latitude grid and then averaged to each OMI ground pixel. The grid points were weighted based on the instrument's spatial sensitivity within the pixel boundaries ~~(Dobber et al., 2006; Kurosu and Celarier, 2010)~~, in contrast to other ~~regional~~custom retrievals, where each grid point was given equal weight ~~(Russell et al., 2011; Lin et al., 2014)~~.

We recalculated temperature correction coefficients $\alpha_k(T_k)$, box AMFs m_k and partial VCDs V_k . The temperature correction coefficients $\alpha_k(T_k)$ were calculated by ~~the empirical~~ Eq. (3) from the WRF/CMAQ output. The box AMFs were computed with the SCIATRAN radiative transfer model. The partial VCDs were also calculated from the WRF/CMAQ output. As an example, two NO₂ profiles are shown in Fig. 2. ~~In contrast to other regional retrievals, we used three-hour means instead of monthly means.~~

3.3.1 Surface reflectance

The surface reflectance was calculated from the MODIS MCD43C2 ~~BSA~~ product. The product is available every eight days compiled from 16 days of ~~measurements~~[data](#). The spatial resolution is $0.05^\circ \times 0.05^\circ$ (Wanner et al., 1997; Lucht et al., 2000). We calculated the ~~BSAs~~[black-sky albedo \(BSA\)](#) from the polynomial representation of the bidirectional reflectance distribution function (BRDF) using solar zenith angle (SZA) and model parameters for MODIS Band 3 (Lucht et al., 2000). MODIS Band 3 has a wavelength range from 459 to 479 nm and a centre wavelength of 470 nm. This band is closest to the DOAS fitting window used in the NO₂ retrieval (405–465 nm). Systematic errors due to the wavelength inconsistency are expected to be small. ~~Over water, Lambertian equivalent reflectance (LER) has been reported to decrease from 440 to 470 (Kleipool et al., 2008; Zhou et al., 2010). We actually find increased BSA over water surfaces in the PRD region. The MODIS BSA~~[The MODIS surface reflectance](#) has been used in other ~~regional~~[custom](#) OMI NO₂ products (~~Zhou et al., 2010; Russell et al., 2011; Lin et al., 2014~~) ([Zhou et al., 2010; Russell et al., 2011; Lin et al., 2014; McLinden et al., 2010](#)).

Since the BSA model parameters have missing values due to cloud contamination, Zhou et al. (2010) filled the data gaps by applying a series of spatial and temporal interpolations. They also reduced measurement noise by applying a smoothing filter. In this work, we combined their steps by using normalised convolution which is a useful algorithm for filling missing values (Knutsson and Westin, 1993). We used a three-dimensional, uniform kernel of size 5 to fill the gaps in the model parameters. ~~To calculate the BSA~~[The BSA was calculated from the model parameters](#) for each OMI ground pixel, ~~the interpolated BSA model parameters were also projected on the longitude-latitude~~[grid](#).

3.3.2 Aerosols and clouds

Scattering by aerosols and clouds affects the AMF (~~Lin et al., 2014~~) ([Leitão et al., 2010](#)). Aerosol scattering ~~enhances the AMF, if aerosols are located below or at the same height as the~~[at or below an](#) NO₂ layer. ~~On the other hand, aerosols scattering reduces the AMF, if aerosols are located~~[increases](#) ~~the AMF, but scattering~~ above the NO₂ layer [will reduce the AMF](#). In addition, aerosol optics ~~affect~~[affects](#) the retrieval of cloud properties.

Clouds are typically handled by the independent pixel approximation (Eq. 4), while aerosols are ~~treated only implicitly in all global and most regional~~ only treated implicitly in the standard and most custom NO₂ products. In ~~SP2, cloud fraction and pressure are~~ OMNO2, cloud pressure and CRF are ~~taken~~ from the OMI O₂–O₂ cloud product which is sensitive to weakly absorbing aerosols (Boersma et al., 2011). Aerosols are also included ~~by the OMI LER in the~~ OMI surface climatology which includes ground haze and persistent cloud features (Kleipool et al., 2008). Lin et al. (2014) included aerosols from a regional GEOS-Chem simulation. They used aerosol optical thickness (AOT) and assumed different profiles of aerosol extinction and absorption coefficients. They also recalculated the OMI cloud product to remove the aerosol component ~~from the product. In a different study,~~ Boersma et al. (2011) derived an empirical relationship between MODIS AOT and OMI ~~aerosol/cloud fraction~~ w:CRF:

$$\underline{w}CRF = 0.21 \cdot AOT. \quad (5)$$

The formula was derived from ~~cloud free~~ observations over North America which were cloud free according to the MODIS AOT retrieval but had non-zero CRF according to the OMI retrieval.

In ~~our study~~ the HKOMI retrieval, we treated clouds as in ~~SP2-OMNO2~~ using the independent pixel approximation. In SCIATRAN, clouds were implemented as an opaque surface at the height of the OMI cloud pressure product with a surface reflectance of 0.8 and the box AMF was calculated with Eq. (4).

Aerosol extinction coefficients can be calculated from the CMAQ output using the empirical IMPROVE formula (Malm et al., 1994). ~~By default~~ In the standard output, CMAQ calculates ~~the only~~ ground level extinction coefficients. In ~~the HK-our custom~~ retrieval, we ~~tested~~ implemented four different aerosol parametrizations:

Case 1: No explicit aerosol treatment, i.e. aerosols were only included implicitly through the OMI cloud product.

Case 2: Aerosols were described by the LOWTRAN aerosol parametrization which requires only very limited information about season, aerosols type, visibility and relative humidity at four different layers: planet boundary layer (PBL) (0–2 km), troposphere (2–10 km), stratosphere and mesosphere. We set the season to autumn/winter and the aerosol type to urban. The PBL visibility was calculated from the CMAQ ground extinction coefficients β using the definition of the meteorological optical range (MOR) (World Meteorological Organization, 2008):

$$MOR = -\frac{\log 0.05}{\beta}. \quad (6)$$

The visibility in the free troposphere was set to 23 km. Furthermore, we assumed that no volcanic aerosols were in the stratosphere or mesosphere. The relative humidity in the

PBL and the free troposphere were taken from WRF. Visibility and relative humidity were set to the nearest predefined value in the LOWTRAN parametrisation.

405 Case 3: Vertical profiles of extinction coefficients β were computed from CMAQ output using the IMPROVE formula. The formula includes a constant Rayleigh extinction coefficient of 0.01 which is subtracted to obtain the aerosol extinction coefficient β_{ext} . Since the IMPROVE formula calculates β_{ext} at 550 nm, an Ångström exponent α for urban aerosols is used to calculate extinction coefficients at 435 nm (Hess et al., 1998). Furthermore,
410 a single scattering albedo ω_0 of 0.82 (urban aerosol) in PBL (below 2 km) and 0.93 in free troposphere is used to calculate aerosol absorption coefficients β_{abs} . The phase function is modelled by Henyey–Greenstein parametrisation with an asymmetry factor g of 0.689 (Hess et al., 1998). As examples, two β_{ext} profiles are shown in Fig. 2.

Case 4: Since ~~this~~ these three parametrisations include aerosols ~~implicitly~~ implicitly through the cloud product, aerosol might be counted twice. Therefore, the CRF was corrected by
415 Eq. (5) using the AOT in CMAQ. This was done mainly because recalculation of the OMI cloud product was outside the scope of our study. Since this formula was derived from cloud free observations over North America, generalisation to cloudy pixels in other regions should be considered with great caution. Otherwise, aerosols were treated as in
420 Case 3.

3.3.3 ~~Application to OMI SP2~~ NO₂ datasets for the PRD region

~~The ancillary parameters were used to calculate new AMFs for all OMI measurements within the PRD region. We created four~~ For our study, we created six OMI NO₂ datasets (PRD-1 to PRD-4) for the four aerosol/cloud cases. The first dataset uses the OMNO2 standard product (OMNO2-SP). For
425 the second dataset (OMNO2-SW), AMFs were recalculated using OMNO2 scattering weights and CMAQ NO₂ profiles. The remaining four datasets were created with our HKOMI retrieval for each aerosol case (HKOMI-1, -2, -3 and -4).

~~While OMI provides daily global coverage, the number of sufficient measurements~~ The number of
OMI NO₂ VCDs, which allows for the study of the NO₂ distribution, is limited due to two factors.
430 Firstly First, the ground pixel size at the end of the swath is very large and thus not suitable for studying the local spatial distribution. Therefore, only the inner fifty out of sixty rows were used in this study. Secondly Second, the presence of clouds increases the retrieval uncertainty. Therefore, only ground pixels were used with ~~aerosol/cloud radiance fractions~~ CRFs smaller than 50 %. Since the CRF is also sensitive ~~aerosol to aerosols~~, this filter criterion is likely to remove heavily polluted
435 days as well. We further removed all orbits that did not have valid pixels in the urbanised area of the model domain (see Fig. 1).

~~Based on these filtering constraints, orbits were picked which have a sufficient number of ground pixels to study~~

3.4 Data processing

440 The OMI NO₂ datasets have been compiled in the instrument's frame of reference (level 2). For comparison and visualisation, the datasets need to be projected to the model grid (level 3) using a suitable gridding algorithm. This is not a trivial task, because the algorithm should conserve the NO₂ VCDs within the OMI ground pixels which are overlapping in along-track direction. In this study, we use a new gridding algorithm which reconstructs the
445 spatial distribution of in PRD region. The orbits were projected using a parabolic spline surface (Kuhlmann et al., 2014, the source code was downloaded at <https://github.com/gkuhl/omi>). Each orbit was projected to a 0.01° × 0.01° longitude-latitude grid. It would be more plausible to project all data to the CMAQ model grid, but the gridding algorithm code currently only supports longitude-latitude grids.

450 Since OMI has a lower spatial resolution than the CMAQ simulation, the satellite instrument cannot resolve small features in the simulated NO₂ distribution. In addition, OMI's spatial resolution depends on the current satellite orbit and thus changes from day to day. Therefore, we create a processed CMAQ dataset (CMAQ processed) from the model output (CMAQ raw). The raw CMAQ VCDs were averaged for each OMI ground pixel in an orbit. Then, the CMAQ data were projected
455 back onto a 0.01° × 0.01° longitude-latitude grid using the ~~same gridding algorithm which has been used to grid~~ gridding algorithm (Kuhlmann et al., 2014). In this step, missing OMI pixels were also removed from the CMAQ data (Kuhlmann et al., 2014). Using this approach, the NO₂ horizontal distributions of OMI and CMAQ are directly comparable.

~~At each ground stations~~ For each RAQM ground station location, time series of tropospheric NO₂
460 VCDs were ~~extracted from the data~~ computed from the six OMI datasets. To study the additive and proportional differences, the OMI VCDs were converted to mixing ratios using the CMAQ NO₂ profile shapes. Since many stations are located on top of buildings, the mixing ratios were calculated at the station height using nearest-neighbour interpolation. In addition, these time series were also computed for the processed CMAQ dataset.

465 ~~Finally, we used a standard set of typical ancillary parameters (Table 1) to study~~

3.5 Evaluation study

For our evaluation study, we have six OMI datasets, two CMAQ datasets as well as time series of these datasets at each RAQM station and the measurements of the RAQM stations. Furthermore, we have simulated and measured meteorological parameters at three ground stations. In this paper, we
470 performed the following analyses with these datasets:

- 475
- ~~First, we compared the six OMI datasets (level 2) with each other to identify the impact of the ancillary parameters on the AMF and thus the tropospheric NO₂ column densities. VCDs. We calculated normalised mean bias (NMB) and coefficient of variance (CV) for all valid OMI VCDs in the datasets. Since high NO₂ values are particularly important for air pollution studies, we also calculated NMB and CV for the 10% highest VCDs based on HKOMI-3. Furthermore, we used a standard set of typical ancillary parameters (see Table 1) to obtain a better understanding of the differences between the datasets.~~

4 Results and discussions

480 ~~In this section, we demonstrate and discuss the results of our study. Firstly, we compare briefly the HK retrieval with SP2 to discuss the influence of the updated ancillary parameters. Secondly, we validate~~

- ~~Second, we compared the WRF/CMAQ simulation using time series with the ground network measurements using index of agreement (IOA), Pearson's correlation coefficient r , root mean square error (RMSE), mean bias (MB), CV and NMB (Table 2). In our analysis, we concentrated on two large urban areas which have the highest NO₂ mixing ratios. The first area consists of the Hong Kong area and the Shenzhen prefecture (HKSZ) and the second area consists of the Foshan and Guangzhou prefectures (FSGZ). HKSZ includes the RAQM stations Liyuan, Tap Mun, Tung Chung and Tsuen Wan. FSGZ includes the RAQM stations Huijingcheng, Luhu Park, Shunde Dangxia and Wanqingsha.~~

- 490
- ~~Third, we validated the RAQM network. Then, we validate the OMI datasets using the RAQM network. Finally, the OMI (level 3) with ground measurements. The validation with point measurements is challenging, because OMI measures the mean value within the ground pixels ($> 13\text{ km} \times 24\text{ km}$). Since NO₂ datasets and CMAQ has a high spatial variability, area average and point measurement may not agree well; in particular in an urban area with complex NO₂ sources and sinks. In order to get an idea for the expected deviations, we compared the time series of the processed CMAQ dataset, which have been averaged to the OMI ground pixels, with the raw CMAQ dataset at the 16 stations. Furthermore, if the VCDs are converted to ground values with the CMAQ profile shapes, the validation depends on the modelled NO₂ profiles which can have large uncertainties. This was studied by comparing different NO₂ profiles.~~
- 500

- ~~Finally, OMI and CMAQ datasets were compared to evaluate the regional chemistry transport model using the HK CTM with the OMI NO₂ datasets. products. We studied the spatial distribution of tropospheric NO₂ VCDs in all datasets. Furthermore, time series were analysed for the two urban areas (HKSZ and FSGZ).~~

4 Results

4.1 OMNO2 and HKOMI NO₂ retrieval

In this subsection, we compare the global product (SP2) with our HK retrieval. Only difference relevant for the later discussion in this paper are described here. For a detailed discussion on the different ancillary parameters, we like to refer the reader to earlier studies and reference therein (Zhou et al., 2010; Russell et al., 2011; Lin et al., 2014).

In our study period, look at the differences between the six OMI NO₂ datasets. After cloud filtering, 56 days (46 of all days) with sufficient OMI data were available. Two examples of ungridded days with satellite observations were available covering about 50% of all days in our study period. Figure 3 shows two examples of tropospheric NO₂ VCDs are shown in Fig. 3. distributions (level 2). The spatial distributions are similar for all products but differences can be seen in a pixel-by-pixel comparison. Particularly evident is that the between the OMNO2-SP, HKOMI-1 and HKOMI-4 datasets with some differences between individual pixels. On the other hand, NO₂ VCDs in the HK retrieval have larger maximum values than in the standard product.

The four-month mean distributions are shown in Fig. magnitudes are quite different between the datasets. Figures 4c and e. The SP2 show the averaged NO₂ distribution for whole study period. The averaged OMNO2-SP dataset has a mean value of 0.4×10^{16} 0.45×10^{16} cm⁻². The mean values in the four datasets range from 0.6 to 0.7×10^{16} and a maximum value of 3.46×10^{16} cm⁻². The smallest mean value has PRD-1 and the largest has PRD-2. PRD-3 and PRD-4 lie in between these extreme cases. The maximum value in the distribution of SP2 is about 3.5×10^{16} , while the HKOMI-4 dataset has a mean value of 0.59×10^{16} cm⁻² and a maximum value of 5.04×10^{16} cm⁻² while the HK retrieval datasets have maximum values ranging from 4.5 – 5.5×10^{16} . The HKOMI-2 dataset has the largest mean (0.70×10^{16} cm⁻²) and maximum value (5.50×10^{16} cm⁻²). Table 3 shows NMB and CV between the datasets for all and the 10% highest VCDs.

To study the difference without explicit aerosol treatment we compare SP2 and PRD-1. For this dataset, the VCDs are increased by (27 ± 39) . The difference are due to the updated ancillary parameters, mainly surface reflectance and profile shapes, and thus due to the recalculated AMFs. For SP2, the mean AMF of all available pixels is 1.01 while the mean AMF of PRD-1 is about 1.17. Since we compared datasets which only differ by one ancillary parameter, the comparison shows the influence of each parameter. CMAQ NO₂ profiles and MODIS surface reflectance increase VCDs by about 10%. When aerosols were included, VCDs increased between 6 and 24% depending on the parametrisation. If a priori profiles and aerosols are replaced, the increase of the VCDs is larger for

the 10% largest VCDs. The HKOMI-4 datasets is $31.0 \pm 34.0\%$ smaller (AMF = 0.83) larger than the OMNO2-SP dataset.

To quantify the impact of the high-resolution profile shapes on the AMF calculation, we compare the CMAQ profiles with an annual GEOS-Chem profile. In order to assess the differences better, we looked at the influence of the ancillary parameters using typical values. Figure 2 shows a “clean” and “polluted” NO₂ profiles from CMAQ and a profile from GEOS-Chem ($2^\circ \times 2.5^\circ$ spatial resolution) which was used for a satellite validation study in for Hong Kong (Chan et al., 2012). The profile was linearly interpolated and extrapolated to the CMAQ vertical levels. The three profiles (see Fig. 2) have been used to compute AMF for the standard case without aerosols (Table 1). The “polluted” CMAQ NO₂ profile has an AMF of 0.82 and is about 3% smaller than the “clean” profile (AMF = 0.84). The GEOS-Chem profile has an AMF of 1.19 which is 41% larger than the “clean” and 45% larger than the “polluted” CMAQ profile. The difference results from the different relative profile shapes. In the CMAQ profiles, the number density decreases with altitude, while the GEOS-Chem profile is nearly constant above 2. The different profile shapes are related to the different vertical advection schemes used in both models. We expect that the regional CMAQ model provides more accurate vertical distributions than the global GEOS-Chem model. The impact of uncertainties in the profile shapes is difficult to quantify because the uncertainties are not well known due to the lack of profile measurements (?). Therefore To determine the variance of the AMFs, we calculated a distribution of AMFs using the simulated profiles at each ground pixel using the standard case. The mean AMF is 0.89 with a SD of 0.08. The the AMFs using all CMAQ profiles. In this sample, the largest AMF is 1.64 as a result of, due to an elevated NO₂ layer in the upper troposphere. The, and the smallest AMF is 0.75 which is 16% smaller than the mean AMF. The small AMF is the result of, due to a heavily polluted ground layer. In summary, the AMF for the high-resolution profiles is about $(35 \pm 11)\%$ smaller than the low-resolution profile.

The profile shapes can also be used to convert VCDs to number concentrations or mixing ratios. For the standard case, the mean conversion factor ($V_0 / (\Delta z_0 V_{\text{top}})$) is $(1.47 \pm 0.47) \times 10^{-3}$ using all available profiles. Therefore, the uncertainty is about 32. The conversion factor of the “clean” and “polluted” profiles are 1.44 and 1.47×10^{-1} , respectively, which is a difference of about 3. The GEOS-Chem profile has a conversion factor 3.92×10^{-3} because of the different profile shape. The sample mean is 0.89 with a standard deviation of 0.08 (about 9% of the mean).

The impact of the surface reflectance can be quantified easier. The mean MODIS BSA is shown Figure 5a shows the MODIS surface reflectance for a SZA of 48° in Fig. 5a. On average, the MODIS BSA is about reflectance is 0.01 ± 0.02 smaller than the OMI LER reflectance (not shown). The BSA is smaller than LER the OMI climatology over land but larger over water. The AMF sensitivity to uncertainties in the surface reflectance depends strongly on the surface reflectance itself (Fig. ??). For the mean surface reflectance (BSA = 0.05) the sensitivity is about 0.06. Therefore, the AMF is reduced by 5 to 10 if the OMI LER product is replaced by MODIS BSA. To In order to

identify the improvement due to the higher spatial ~~and temporal~~-resolution, we averaged the BSA to the lower spatial resolution used in the ~~global standard~~ product ($0.5^\circ \times 0.5^\circ$). ~~Then, we and~~ subtracted the high-resolution BSA used in our ~~regional custom~~ product (Fig. 5b). The distribution shows areas with large differences (up to ± 0.03) along the urbanised and likely polluted coastline ~~As a result, if we assume an AMF of 0.83, the retrieval error, due to a low spatial resolution, can be locally as large as which would result in large biases (up to $\pm 20\%$ for a reflectance of 0.05) in the AMF calculation.~~

~~The differences between PRD-1 to PRD-4 are due to the different aerosol treatments. Table 4 shows the AMFs for the different aerosol cases using the “clean” and “polluted” profiles in (Fig. 2 and the standard parameters (Table 1). PRD-3 and PRD-4). Cases 3 and 4 are equal because the standard parameter assume cloud free conditions. If aerosols are included, the AMF is reduced because the aerosol is located above the layer (Fig. 2).~~

~~In PRD-2, the CRF is zero in the test parameters. The Case 2 AMFs are 19% smaller than Case 1 for the “clean” and 57% smaller for the “polluted” aerosol profile. If Case 3 is compared to Case 1, the AMF is reduced between 8 and 14% (Table 4). In Case 2, the CMAQ ground level extinction coefficient is used as constant coefficient in the PBL (0-20-2 km). If PRD-2 is compared to PRD-1, the AMF is reduced by 19 for the “clean” and by 57 for the “polluted” aerosol profile (Table 4). The β_{ext} profiles in Fig. 2 show that using the ground level extinction coefficient is reasonable for a “clean” b_{ext} profile but not for a “polluted” profile. In the latter case, profiles (Fig. 2), because β_{ext} would be overestimated between is overestimated above 1 and 2 km and thus reduce which reduces the AMF because these aerosols are located above artificial aerosols are shading the NO_2 layer. As consequence, the ground level extinction coefficient should not be used as PBL mean value for “polluted” cases, because this assumption can severely overestimate the column densities. below.~~

~~PRD-3 and PRD-4 use a b_{ext} profile calculated with the IMPROVE formula. The b_{ext} profiles have a maximum value at about 500 above ground which correlates with the maximum relative humidity. The shape of the profiles is in reasonable agreement with LIDAR measurements in Hong Kong (He et al., 2008). However, the formula was not developed to calculate profiles in an urban environment and thus should be treated with caution. If PRD-3 is compared to PRD-1, the AMF is reduced between 8 and 14 (Table 4).~~

~~If aerosols are included, PRD-4 is likely to be the most reasonable assumption. The mean difference between VCDs in SP2 and PRD-4 is (-31 ± 38) . The difference between PRD-1 and PRD-4 is $(+4 \pm 11)$ showing a large impact due to aerosols. The difference between PRD-4 and PRD-3 is $(+1 \pm 7)$.~~

~~To conclude, our regional datasets have higher VCDs than the global product (SP2) because of updated ancillary parameters. On the local scale, systematic errors should be reduced because of the higher spatial resolution.~~

4.2 WRF/CMAQ validation with ground measurements

In this section, the WRF/CMAQ model is evaluated with ground measurements of meteorological observations and the PRD RAQM network. The errors measures used on the validation are summarised in the appendix.

4.2.1 Temperature, humidity, pressure and wind

The results of the validation are shown in the Supplement. The index of agreement (IOA, see Appendix ??)

The results of the WRF validation with the automatic weather stations are tabulated in the Supplement (Tab. S1). The IOA between observed and simulated sea level pressure is high (IOA = 0.99) at all stations. Simulated temperature and humidity also agree well have high agreement with the observations. The model slightly underestimates temperature and humidity over land (at HKO and HKIA). The model also overestimates humidity on Waglan Island where the model data are at the sea surface while measurements were taken at station height of 56 over the sea surface.

Since the wind field is impacted strongly by local topography, the agreement between model and observation is normally lower where the topography is complex and thus cannot be resolved by the model. The Hong Kong Observatory uses Waglan Island as reference station because it is not influenced by local topography. The agreement between model and observations on Waglan Island is good, while it slightly overestimates temperature and humidity at WGL. The agreement between modelled and observed wind speed is highest at WGL (IOA = 0.84). At HKIA the wind field is impacted by the mountainous Lantau Island and thus the agreement is lower, which is located on a remote island, and lower at HKIA (IOA = 0.68). The HKO station is located within urbanised Kowloon and surrounded by high buildings. Consequently, the agreement between model and observations is low and HKO (IOA = 0.57), which are located in complex terrain.

The evaluation of the meteorological fields shows good agreement between model and observations within the expected limitations due to the model resolution. The agreement is lower for the wind fields due to the impact of local topography. Unfortunately no meteorological data for the whole PRD region were available for this analysis. However, due to the high agreement in Hong Kong, similar model performance is expected in the complete model domain. The meteorological fields are sufficient to provide input for the chemistry transport simulations.

4.2.1 mixing ratios

The results of the statistical evaluation between CMAQ and CMAQ validation with the RAQM network are summarised tabulated in the Supplement (Tab. S2). For the sixteen stations, the index of agreements IOAs have an average of 0.52 and vary between 0.29 and 0.75. At most stations the IOA is about 0.5. At Tap Mun, the low IOA is the result of several peaks in the simulated time

series which are not found in the measurements. The peaks were traced back to emissions at the Dapend Peninsula about 15 east of Tap Mun (not shown). Other stations in Hong Kong have IOA above average.

There are various reasons for the disagreement between model and measurements. Firstly, the point measurement may not be representative for the grid cell because of the influence of local sources and sinks. Secondly, local topography and station height can also impact the mixing ratios. On the other hand, the differences can arise from the model due to the limited parametrisation of the chemistry and in particular the insufficient knowledge of the strength and distribution of the emissions.

(Tap Mun) and 0.75 (Tsuen Wan). The average ground mixing ratios are shown in Fig. 6. In the observations measurements, two major plumes can be identified at Hong Kong and Shenzhen (HK in HKSZ and in FSGZ. In the simulations, the FSGZ plume is much less pronounced than in the measurements, which can be seen in the averaged mean bias which is -17.6 SZ), which includes the network stations Liyuan, Tap Mun, Tung Chung and Tsuen Wan, and Foshan and Guangzhou (FSGZ), which includes the stations Huijingcheng, Luhu Park, Shunde Dangxia and Wanqingsha. The latter plume cannot be found in the simulations. The mean bias is close to zero ppbv (-544 %) at the stations in HKSZ. The bias is larger in FSGZ with a MB of for the four stations in FSGZ. The averaged mean bias is $-17.60.0$ ppbv (-455 %) for the stations in HKSZ.

The better agreement over Hong Kong is thought to be the result of the updated emission inventory with local information from Hong Kong which are more accurate. The low agreement between model and observation is not very satisfying. In another study, Wu et al. (2012) evaluated CMAQ in the PRD region using a similar emission inventory and reported similar CVs (see Appendix ?? for definition) and normalised mean biases. The low model performance can impact the quality of the OMI dataset because the low model performance might reduce the accuracy of the profile shape and thus impact the air mass factor and the conversion factor which is used to convert VCDs to ground mixing ratios.

4.3 OMI validation with ground measurements

In this subsection, OMI columns were compared with the RAQM network. The validation with point measurements is challenging, because OMI measures the mean value within the ground pixels (at least $13\text{ km} \times 24$). Since has a high spatial variability, area average and point measurement may not agree well; in particular in an urban area with complex sources and sinks. Furthermore, if the VCDs are converted to ground values with the CMAQ profile shapes, the validation depends on the modelled profiles which can have large uncertainties.

In order to get an idea for the expected deviations, we compared the time series of the processed CMAQ data, which have been averaged to the OMI ground pixels, with the raw CMAQ data ($3\text{ km} \times 3$) at the 16 stations. The comparison between OMI datasets and RAQM stations is impacted

by the area averaging effect. The expected error measures were computed by comparing raw and processed CMAQ datasets (Table 5 shows the mean error measures for all stations and for the stations within the two plumes. The). The expected correlation coefficient is low, in particular, over HKSZ. This lower agreement in Hong Kong could result from the complex terrain along the coastline and the strong gradient between clean and polluted air (see Fig. 6a). Against that, the distribution in FSGZ is smoother. Table 5 also shows that the processed data have lower mixing ratios with a mean bias between very low ($r = 0.25$) at HKSZ and good ($r = 0.67$) at FSGZ. The expected NMBs are -10% and -20% which is the result of the spatial averaging. The generalisation of these results to the OMI validation should be done with caution because it requires that the model simulates the spatial distribution on a small scale accurately. Nonetheless, this analysis provides some useful information on the expected deviations between satellite and ground measurements 12% at HKSZ and FSGZ, respectively.

To study additive and proportional differences between satellite and ground measurements observations, the OMI VCDs were converted to ground level mixing ratios using the CMAQ NO₂ profile shapes. As an example, the profiles. The mean conversion factor ($V_0/(\Delta z_0 V_{top})$) is $(1.47 \pm 0.47) \times 10^{-3} \text{ m}^{-1}$. The conversion factor of the “clean” profiles is about 3% smaller than of the “polluted” profile. The GEOS-Chem profile has a conversion factor of $3.92 \times 10^{-3} \text{ m}^{-1}$ which is more than twice the factor computed for the CMAQ profiles. As a result, ground level mixing ratios would be much larger if the GEOS-Chem profile would be used for the conversion. The ground mixing ratio distribution for 29 January 2007 map is shown in Fig. 7 using a “standard” and the newly developed gridding algorithm. The new algorithm creates continuous distributions which is helpful for the study of the spatial distribution distribution. It should be noted that the high-resolution features are the result of modelled profile shapes. Therefore, the ground mixing ratios depend strongly on the for 29 January 2007 using two different gridding algorithms. The algorithm which uses parabolic splines does not show discontinuities at the pixel boundaries and has slightly larger VCDs (Fig. 7b). The NO₂ profile shape in the variability below the OMI pixel size is caused by the variability of the CMAQ profile shapes showing the large impact of the model.

Table 6 shows the statistical measures for the comparison between OMI the six OMI datasets and the ground network for SP2 and datasets using the HK retrieval. The. Statistical measures for all 16 stations are tabulated in the Supplement (Table S3) showing that the measures vary considerably between the stations. The averaged correlation coefficients are similar for all datasets. The size of the correlation coefficient is comparable to the expected values with no large difference between the datasets. At FSGZ, r is smaller than the expected value, while at HKSZ, r is close to the quite small expected value (Table 5). The correlation coefficients is slightly smaller at FSGZ which is likely related to the low model performance in this area.

720 ~~There are large differences between~~ At HKSZ, the HKOMI datasets have a slightly larger correlation coefficient than the two OMNO2 datasets. The datasets largely differ in the mean biases. The bias is largest for the ~~global product (SP2). In the HK retrieval, the mean bias depends on the amount of aerosols. The bias is largest for PRD-1 OMNO2-SP and smallest for PRD-2, while PRD-3 and 4 lie in between them. The magnitude of the HKOMI-2 dataset.~~ The bias is closest to the expected value for PRD-4. ~~The reduced mean bias is an important improvement of the HK bias for the HKOMI-3 and -4 datasets. OMNO2-SP and -SW underestimate NO₂ retrieval, mixing ratios while HKOMI-2 overestimates the mixing ratios.~~

4.4 CMAQ evaluation with OMI NO₂ datasets

730 The modelled NO₂ VCDs were evaluated with the OMI NO₂ datasets. Figures 4a and b show the difference between the raw and the processed CMAQ dataset. In the processed dataset, the spatial NO₂ distribution is smoothed below the size of the OMI ground pixel. Therefore, CMAQ (processed) and OMI datasets can be directly compared without artefacts due to different spatial resolutions.

735 Table 7 shows the mean values of CMAQ, OMI datasets and RAQM network at the location of the 16 stations at RAQM stations for CMAQ and OMI datasets. If the local distribution was simulated perfectly, the raw CMAQ data would agree model performance would be good, CMAQ (raw) should agree well with RAQM and CMAQ (processed) should agree well with the network measurements and the processed CMAQ data would agree with the OMI measurements. However, the bias between OMI PRD-4 and RAQM network at FSGZ is larger than the expected value. The difference is likely the result of the CMAQ model bias in this area. If we compare the “clean” and “polluted” standard case (Table 1), the different profile shape (3 datasets. The former were already compared in Sect. 4.2.1 showing a small bias at HKSZ and a large bias at FSGZ. The results are similar between CMAQ (processed) and HKOMI-4 having similar mean values at HKSZ but a large bias at FSGZ.

745 The NO₂ distribution of the HKOMI-4 dataset has one plume at FSGZ and a second plume at HKSZ (Fig. 4e). In addition, the OMI dataset has increased NO₂ near the northern edge of the model domain and at the Pearl River in the western part of the domain. The differences between CMAQ and OMI are shown in Fig. 4d and f. The modelled VCDs are underestimated at FSGZ and overestimated at HKSZ. The form of the plume at HKSZ differ between OMI and CMAQ. In CMAQ, the plume has an elliptic shape with a strong, south-western outflow. In the OMI datasets, this feature is less distinct.

750 The results of the time series analysis are shown in Table 8. The correlation coefficient is smaller at FSGZ than at HKSZ. At FSGZ, CMAQ VCDs are much smaller than the HKOMI-4 VCDs (NMB = -40 %), conversion factor (-). This bias is close to the bias between CMAQ and RAQM (-344 %) and the influence of the aerosols (-10). On the other hand, CMAQ VCDs are larger than

the OMI VCDs (+15%) can increase the AMF by 10 to 20 (see Sect. 4.1). As a result, the OMI VCDs would be larger and the bias between OMI and network would become smaller.) at HKSZ.

755 To conclude, the correlation coefficient between all OMI datasets and ground measurements is low. The low correlation is mainly related to the OMI ground pixel size as well as to the unsatisfactory performance of the CMAQ model. However, the HK retrieval reduces the mean bias between satellite and ground measurements significantly. The larger bias in FSGZ suggests that OMI VCDs might be still underestimated in the HK retrieval (PRD-4) due to the model bias in this region.

760 5 Discussions

5.1 CMAQ evaluation with OMI datasets in the model domain

In this subsection, we compare the OMI datasets with the CMAQ data. We discuss mainly PRD-4 which performed best in

5.1 Influence of ancillary parameters

765 Ancillary parameters have a large influence on the retrieval of tropospheric NO₂ VCDs. In our study, their influence on the AMFs is similar to findings for other retrieval algorithms (e.g. Zhou et al., 2010; Russell et al., 2011; Lin et al., 2014). A direct comparison is difficult because the influence depends on regional factors. For example, we found a very strong gradient in surface reflectance along the coastline in the PRD region which has a large influence on tropospheric
770 NO₂ VCDs. In other regions, the variability of surface reflectance can be smaller influencing VCDs less.

In our retrieval, CMAQ NO₂ profiles were used which have a quite different shape compared to GEOS-Chem profiles (Fig. 2). Since NO₂ profile measurements were not available for the PRD region, the modelled profiles were not validated in this study. As a consequence, AMF
775 uncertainties due to NO₂ profiles are difficult to quantify. However, it can be argued that the regional CMAQ CTM provides more accurate vertical distributions than the global model, because of higher spatial resolution and more detailed PBL, vertical advection and diffusion schemes. On the other hand, different schemes exist for regional CTM and these might result in different NO₂ profiles (e.g. Tang et al., 2011; Xie et al., 2012). Therefore, the validation of
780 model profiles is important to better estimate the uncertainties for model evaluation with satellite observations. In this study, the ~~validation~~ CMAQ NO₂ profiles have a strong vertical gradient in the PBL which is expected for strong emissions near the surface. The qualitative shape of the profile agrees reasonable with measured and simulated urban NO₂ profiles used in other studies (e.g. Schaub et al., 2006; Leitão et al., 2010).

785 Aerosols have a large influence on the retrieved VCDs. In the HKOMI retrieval, good agreement
with ground measurements. ~~Since the correlation between OMI and RAQM network is low, only
spatially or temporally averaged distribution were compared which reduces the random noise.~~

~~Figure 4a-c and e shows the four-month averaged CMAQ and OMI was found when calculating
 β_{ext} profiles and reducing CRF based on AOT in the model (Case 4). β_{ext} calculation and~~
790 ~~CRF reduction are based on empirical formulas which have the advantage that they are easy to
use. However, the IMPROVE formula was not developed to calculate β_{ext} profiles in an urban
environment which can result in uncertainties. An improved IMPROVE formula is available which
we consider to use in an updated version of our retrieval (Zhang et al., 2013). Alternatively,
optical properties can be calculated by Mie theory. The aerosol information was not validated with~~
795 ~~ground- or satellite observations which is also planned to be implemented in an updated version.
Nevertheless, the shape of the aerosol profiles is in reasonable agreement with LIDAR measurements
in Hong Kong (He et al., 2008). The empirical cloud correction formula is also very simple and, as
mentioned before, should be improved in future. In conclusion, the impact of aerosols and clouds
is an important factor for unbiased retrieval of tropospheric NO₂ VCDs. The averaged raw CMAQ
800 data and the processed CMAQ data are shown Fig. 4a and b. Some high-resolution features, which
cannot be resolved by OMI, are smoothed in the processed. Unfortunately, a complete treatment of
aerosols and clouds is complex and often not feasible for air quality model evaluations.~~

The OMI surface reflectance climatology provides scene reflectance, which includes both the
surface and the presence of boundary layer haze or aerosols, and minimum reflectance, which is
805 the lowest retrieved reflectance value (Kleipool et al., 2008). ~~Since scattering by weakly-absorbing
aerosols at or below an NO₂ distribution. Since the OMI lattice changes with each orbit, this
processing also provides an easy way to distinguish features which can and cannot be resolved
by the current orbit~~layer increases AMFs, it has been argued that scene reflectance should
be used for satellite-based trace gas retrieval, if no information about aerosols are available
810 (Herman et al., 2001). Furthermore, the minimum reflectance can be underestimated due to ground-
and cloud shading or darkening by rainfall. For these reasons, scene reflectance is used in the
standard product (Boersma et al., 2011). However, if an NO₂ layer is mixed with highly-absorbing
aerosols, the AMF is not increased but decreased (Leitão et al., 2010). In the HKOMI retrieval, we
have highly-absorbing ($\omega_0 = 0.82$), urban aerosols and thus AMFs are decreased in the presence
815 of aerosols. As a result, if scene reflectance is used for an urban area, NO₂ VCDs can be strongly
underestimated.

Since ancillary parameters have a large influence on the VCDs, it is important to quantify their
uncertainties. This is often difficult because vertical profiles are required which are rarely available.
In the view of model evaluation, it is also helpful if surface reflectance, aerosols and clouds are
820 provided independently, because it allows to use modelled aerosol profiles in the retrieval.

The differences between CMAQ and OMI are shown in Fig. 4d and f. The two major plumes at Foshan and Guangzhou (FS

5.2 WRF/CMAQ validation with ground measurements

The evaluation of the meteorological fields shows good agreement between model and observations within the expected limitations due to the model resolution. The agreement is lower for the wind fields due to the impact of local topography. Unfortunately no meteorological data for the whole PRD region were available. However, due to the high agreement in Hong Kong, similar model performance is expected in the complete model domain. The meteorological fields are sufficient to provide input for the chemistry transport simulations.

The agreement between CMAQ and RAQM network is low for various reasons. First, the point measurement may not be representative for the grid cell because of the influence of local sources and sinks as well as local topography and station height. Second, the differences can arise from the model due to inaccurate wind fields, limited parametrisation of the chemistry and, in particular, insufficient knowledge about strength and distribution of emissions. The model performance is similar to the result by Wu et al. (2012) who also evaluated CMAQ in the PRD region using a similar emission inventory.

The low model performance can largely be explained by problems with the emission inventory. For example, the low IOA at Tap Mun is the result of several peaks in the simulated time series which were not found in the measurements. The peaks were traced back to NO_x emissions at the Dapend Peninsula about 15 GZ) and Hong Kong and Shenzhen (HKSZ) are marked by the left and right box, respectively. For each orbit, OMI and CMAQ VCDs were averaged within the two boxes to create a time series for each plume. The results of the time series analysis are shown in Table 8 and two scatter plots are shown in Fig. ?? km east of Tap Mun. As a second example, the large bias between model and observations at FSGZ is mainly due to underestimated NO_x emissions in this region. The smaller bias in HKSZ is thought to be the result of the updated emission inventory with more accurate information for Hong Kong. It should be noted that updated emission inventories exist for the PRD region which would improve the model performance. However, our objective was not an accurate CMAQ simulation but a model evaluation with satellite observations. For this application, the used emissions inventory was found to be very useful.

At FSGZ, the correlation coefficient is low ($r \approx 0.4$) and the CMAQ VCDs are much smaller than the OMI PRD-4 VCDs ($\text{MB} = -40$

5.3 OMI validation with ground measurements

The OMI datasets were validated with the RAQM network. The HKOMI retrieval does not change the correlation coefficient considerably compared to the standard products, while they are generally increase in other custom products (e.g. Lin et al., 2014; Russell et al., 2011; Zhou et al., 2009). The

non-existent improvement has two main reasons. First, the low CTM performance can result in random errors impacting ancillary parameters and conversion factors. Second, ground-based point values were compared with satellite-based area-averaged values in an urban area with high NO₂ variability. The expected discrepancies between ground- and satellite-based observations were estimated using CMAQ NO₂ distributions showing that the expected correlation coefficients were quite small reducing possible improvements.

On the other hand, the HKOMI retrieval significantly reduces the bias between ground- and satellite-based observations. However, systematic errors in the parameters can still cause biases in the datasets. For example, if the model underestimates emissions, NO₂ and β_{ext} profiles might be described better by the “polluted” than the “clean” profiles (Fig. 2). As a consequence, the AMFs are reduced by about 9 %. At HKSZ, the correlation is better ($r \approx 0.6$) and the CMAQ VCDs are larger than the OMI VCDs (+15 conversion factor by about 3 %). These results confirm the CMAQ bias identified in the evaluation with the ground measurements. The model biases between OMI PRD-4 and CMAQ (processed). Therefore, NO₂ mixing ratios would be underestimated by 10 to 20 % which can partly explain the large NMB at FSGZ.

Besides these limitations, the HKOMI retrieval shows the possibility for unbiased NO₂ observations using satellite instruments. Of the four aerosol cases, HKOMI-4 performed best with the highest correlation coefficient and the smallest NMB. Furthermore, HKOMI-4 makes the most reasonable assumptions, although very simple, about aerosols and clouds. Correlation coefficients and mean biases are expected to improve further with better CTM performance.

5.4 Model evaluation and further applications

The model evaluation with OMI NO₂ datasets demonstrated that it is possible to study the spatial distribution and the magnitude of NO₂ VCDs with satellite observations. The biases between CMAQ and HKOMI-4 are consistent with the biases found between RAQM network and CMAQ (raw) (see Table 7). Since the CMAQ distribution has been processed like OMI, no area averaging effects occur in this comparison. The errors in the OMI measurements are mainly due to uncertainties in the ancillary parameters which are mainly taken from the model simulation bias found between CMAQ and RAQM giving us further confidence that the HKOMI-4 retrieval results in smaller systematic errors. Small systematic errors are important for various applications.

The HK retrieval In air quality studies, satellite observations can be used for the study of the spatial to obtain ground level NO₂ distribution. An example is the shape of the plume at Hong Kong. In CMAQ, the plume has an elliptic shape with a strong, south-western outflow. In the OMI datasets, this feature is less distinct. This difference might be caused by the spatial resolution of CMAQ which does not resolve the mountainous Lantau Island (south of Tung Chung, see Fig. 1) concentrations (e.g. Lamsal et al., 2008). To estimate the impact on human health, these concentrations need to be unbiased because otherwise the air quality is misinterpreted. This is particular important in polluted

areas, where NO_2 VCDs can be biased due to the presence of absorbing aerosols. Our retrieval reduces this bias in particular for high NO_2 values making it more suitable for satellite-based air quality studies in urban areas.

895 ~~The OMI measurements~~ Satellite observations can also be used ~~where no ground measurements are available. For example, the OMI measurements show several smaller plumes which are missing in CMAQ. For instance, in the northern and western part of the model domain.~~

~~In summary, the HK retrieval provides a better suited dataset which can be used for the evaluation of the CMAQ model for estimating NO_x emissions by inverse modelling~~
900 ~~(e.g. Mijling et al., 2013; Gu et al., 2014). Systematic errors in the satellite observations can cause biases in the derived emission inventory (e.g. Connor et al., 2008). To reduce this problem, Gu et al. (2014) derived emissions by iteratively updating the a priori NO_2 profiles used in satellite retrieval. Their method reduces differences between emissions derived from GOME-2 and OMI. However, we and other showed that NO_2 VCDs can still be biased due to surface reflectance,~~
905 ~~aerosols and clouds. Therefore, we think it is necessary to also update AKs in the inverse method and to characterise the spatiotemporal distribution of systematic errors in the satellite retrieval. The latter was done, for example, for the retrieval of carbon dioxide (Buchwitz et al., 2013).~~

6 Conclusions

In this paper, we ~~evaluate~~ evaluated biases in a regional CTM ($3\text{ km} \times 3\text{ km}$ spatial resolution)
910 ~~with satellite measurements. We simulated three-dimensional atmospheric chemistry~~ ground- and satellite-based NO_2 observations. Atmospheric chemistry was simulated with the CMAQ modelling system ~~the PRD region from October 2006 to January 2007. Furthermore, we developed a new OMI retrieval for this region. The CMAQ model was evaluated with the global and ground measurements were taken from the RAQM network. Six OMI NO_2 standard product (SP2), our HK retrieval~~
915 ~~using different aerosol parametrizations (PRD-1 to PRD-4), and ground measurements of the PRD Regional Air Quality Monitoring (RAQM) network.~~

~~In the HK datasets were compiled with NASA's standard retrieval (OMNO2-SP and -SW) and our custom retrieval (HKOMI-1 to -4). In the OMNO2-SW dataset, a priori NO_2 profiles were replaced by CMAQ profiles using the scattering weights provided with the product. In the HKOMI~~
920 ~~retrieval, we recalculated tropospheric AMFs using updated ancillary parameters of a priori NO_2 profile shapes~~ profiles, surface reflectance and aerosol profiles. ~~Our best retrieval (PRD-4) increases the~~ The HKOMI datasets differ in how aerosols were implemented in the retrieval.

The updated ancillary parameters increased tropospheric NO_2 VCDs by $(+31 \pm 38 + 11.4 \pm 13.4)\%$, when compared to SP2, and thus reduces the mean bias (a priori
925 NO_2 profiles), $(+11.0 \pm 20.9)\%$ (surface reflectance) and $(+6.0 \pm 8.4)\%$ (HKOMI-4 aerosol parametrization). As a result, the normalised mean bias (NMB) between satellite and ground

measurements significantly (observations was significantly reduced from -15 instead of -41 %
). The differences are due to changes in the ancillary parameters used for the AMF calculation.
These parameters are profile shapes (-35 ± 11), surface reflectance (-5 (OMNO2-SP) to -10 15 %
930) and aerosols (-8 to -14 (HKOMI-4)). The remaining difference between satellite and ground
measurements biases can be explained by the area averaging CMAQ model bias and the area
averaging effect due to the OMI ground pixel size and by the CMAQ model bias because the OMI
retrieval depends on the CMAQ model output. As a result, if the CMAQ model underestimates
mixing ratios or aerosols, the OMI VCDs can be underestimated as well. This relation should be
935 considered in an evaluation study. Replacing only the a priori profiles, which is recommended for
model evaluation studies, only reduced the NMB to -32 %.

In a polluted environment, accurate knowledge of the vertical profiles of aerosol and cloud
scattering as well as Since ancillary parameters have such a strong influence on the VCDs, the
parameters need to be well known to obtain accurate NO_2 profile shapes are important to calculate
940 accurate column densities. Our study is limited by unquantified errors due to uncertainties in the
VCDs and to estimate their uncertainties. In our study, NO_2 profile and aerosol profile. In future
studies, the HK retrieval should be reviewed by validating the CMAQ profiles. Furthermore, the
aerosol optical properties were calculated by the IMPROVE formula which has not been developed
to calculate profiles in an urban environment. However, the IMPROVE formula can be improved
945 for such an application (Zhang et al., 2013) which we like to include in a future version. Otherwise,
optical properties can be calculated by Mie theory. The aerosol information can be improved further
by validating them with ground or satellite-based products. A third aspect is the impact of clouds
which need to be studied more in future. Satellite products, which provide a clean separation between
aerosols, clouds and surface reflectance, are desirable, because this would allow to use different data
950 sources for these ancillary parameters and aerosol profile observations were not available making
it difficult to estimate uncertainties and their impact on the AMF calculations. Future studies are
necessary to address these limitations.

The performance of the model is not very satisfying. The correlation between CMAQ and RAQM
network is low ($r \approx 0.3$) and the model underestimates the concentrations in the north-western
955 model domain (CTM performance was low mainly due to the underestimated emissions causing
a large bias in Foshan and Guangzhou). The low performance is assumed to be associated with
the used emissions inventory, because the model performance is better in Hong Kong and Shenzhen
where the emission inventory has been updated with local data. The ($\text{NMB} = -40\%$). However,
the results the model evaluation with the HK retrieval (PRD-4) gives similar results. In Hong Kong
960 and Shenzhen, the model overestimates the RAQM network and the OMI NO_2 VCDs by about 15,
while the correlation coefficient is satisfactory ($r = 0.56$). In Foshan and Guangzhou, the correlation
is low ($r = 0.37$) and the model underestimates the VCDs strongly ($\text{MB} = -40$). Furthermore, we
estimated that the HK retrieval also underestimated VCDs by about datasets were consistent. We

965 ~~also estimated that our custom retrieval could still underestimate VCDs by 10 to 20 % in Foshan and Guangzhou because of the influence of the model parameters on the AMF. The results of both model evaluations with the RAQM network and the datasets created by the HK algorithm are consistent~~ some areas which is important to remember when validating a model with satellite products. In general, we expect an improved HKOMI product with better CTM simulation.

970 To conclude, our study demonstrates that the datasets created by the ~~HK~~ HKOMI retrieval are suitable for the evaluation of the spatial ~~distribution and the magnitude~~ distributions and the magnitudes of NO₂ concentrations in the model. We showed that a retrieval, which updates not only ~~the profile~~ shapes a priori NO₂ profiles, reduces the ~~OMI bias over~~ biases in urban areas. ~~In future studies, easy-to-use~~ Since the ancillary parameters have a large impact on the retrieval, tools need to be developed ~~which allow such evaluations of CTMs with satellite measurements as easy as using ground~~ network measurements.

975

7 ~~Error measures~~

**The Supplement related to this article is available online at
doi:10.5194/acp-0-1-2015-supplement.**

980 *Acknowledgements.* The work described in this paper is partly funded by the Guy Carpenter Asia-Pacific Climate Impact Centre (project no. 9360126), a grant from the Research Grant Council of Hong Kong (project no. 102912) and the start-up grant from City University of Hong Kong (project no. 7200296).

References

- Acarreta, J. R., De Haan, J. F., and Stammes, P.: Cloud pressure retrieval using the O₂-O₂ absorption band at 477 nm, *J. Geophys. Res.*, 109, D05204, doi:10.1029/2003JD003915, 2004.
- 985 [Beirle, S., Platt, U., Wenig, M., and Wagner, T.: Weekly cycle of NO₂ by GOME measurements: a signature of anthropogenic sources, *Atmos. Chem. Phys.*, 3, 2225–2232, doi:10.5194/acp-3-2225-2003, 2003.](#)
- Bey, I., Jacob, D. J., Yantosca, R. M., Logan, J. A., Field, B. D., Fiore, A. M., Li, Q., Liu, H. Y., Mickley, L. J., and Schultz, M. G.: Global modeling of tropospheric chemistry with assimilated meteorology: model description and evaluation, *J. Geophys. Res.*, 106, 23073–23095, doi:10.1029/2001JD000807, 2001.
- 990 ~~Boersma, K. F., Eskes, H. J., and Brinksma, E. J.: Error analysis for tropospheric retrieval from space, *J. Geophys. Res.*, 109, D04311, doi:, 2004.~~
- Boersma, K. F., Eskes, H. J., Meijer, E. W., and Kelder, H. M.: Estimates of lightning NO_x production from GOME satellite observations, *Atmos. Chem. Phys.*, 5, 2311–2331, doi:10.5194/acp-5-2311-2005, 2005.
- Boersma, K. F., Eskes, H. J., Veefkind, J. P., Brinksma, E. J., van der A, R. J., Sneep, M., van den Oord, G. H. J., 995 Levelt, P. F., Stammes, P., Gleason, J. F., and Bucsele, E. J.: Near-real time retrieval of tropospheric NO₂ from OMI, *Atmos. Chem. Phys.*, 7, 2103–2118, doi:10.5194/acp-7-2103-2007, 2007.
- Boersma, K. F., Eskes, H. J., Dirksen, R. J., van der A, R. J., Veefkind, J. P., Stammes, P., Huijnen, V., Kleipool, Q. L., Sneep, M., Claas, J., Leitão, J., Richter, A., Zhou, Y., and Brunner, D.: An improved tropospheric NO₂ column retrieval algorithm for the Ozone Monitoring Instrument, *Atmos. Meas. Tech.*, 4, 1000 1905–1928, doi:10.5194/amt-4-1905-2011, 2011.
- Bovensmann, H., Burrows, J. P., Buchwitz, M., Frerick, J., Noël, S., Rozanov, V. V., Chance, K. V., and Goede, A. P. H.: SCIAMACHY: mission objectives and measurement modes, *J. Atmos. Sci.*, 56, 127–150, 1999.
- 1005 [Buchwitz, M. and Reuter, M. and Bovensmann, H. and Pillai, D. and Heymann, J. and Schneising, O. and Rozanov, V. and Krings, T. and Burrows, J. P. and Boesch, H. and Gerbig, C. and Meijer, Y. and Löscher, A.: Carbon Monitoring Satellite \(CarbonSat\): assessment of atmospheric CO₂ and CH₄ retrieval errors by error parameterization, *Atmos. Meas. Tech.*, 6, 3477–3500, doi:10.5194/amt-6-3477-2013, 2013.](#)
- Bucsele, E. J., Celarier, E. A., Wenig, M. O., Gleason, J. F., Veefkind, J. P., Boersma, K. F., and Brinksma, E. J.: Algorithm for NO₂ vertical column retrieval from the ozone monitoring instrument, *IEEE T. Geosci. Remote*, 44, 1245–1258, doi:10.1109/TGRS.2005.863715, 2006.
- 1010 Bucsele, E. J., Krotkov, N. A., Celarier, E. A., Lamsal, L. N., Swartz, W. H., Bhartia, P. K., Boersma, K. F., Veefkind, J. P., Gleason, J. F., and Pickering, K. E.: A new stratospheric and tropospheric NO₂ retrieval algorithm for nadir-viewing satellite instruments: applications to OMI, *Atmos. Meas. Tech.*, 6, 2607–2626, doi:10.5194/amt-6-2607-2013, 2013.
- 1015 Burrows, J. P., Weber, M., Buchwitz, M., Rozanov, V., Ladstätter-Weissenmayer, A., Richter, A., DeBeek, R., Hoogen, R., Bramstedt, K., Eichmann, K. U., Eisinger, M. and Perner, D.: The global ozone monitoring experiment (GOME): mission concept and first scientific results, *J. Atmos. Sci.*, 56, 151–175, 1999.
- Byun, D. and Schere, K. L.: Review of the governing equations, computational algorithms, and other components of the Models-3 Community Multiscale Air Quality (CMAQ) modeling system, *Appl. Mech. Rev.*, 59, 1020 51–57, doi:10.1115/1.2128636, 2006.

- Callies, J., Corpaccioli, E., Eisinger, M., Hahne, A., and Lefebvre, A.: GOME-2 – Metop’s second-generation sensor for operational ozone monitoring, *ESA Bull.-Eur. Space*, 102, 28–36, 2000.
- Chan, K. L., Pöhler, D., Kuhlmann, G., Hartl, A., Platt, U., and Wenig, M. O.: NO₂ measurements in Hong Kong using LED based long path differential optical absorption spectroscopy, *Atmos. Meas. Tech.*, 5, 901–912, doi:10.5194/amt-5-901-2012, 2012.
- 1025 [Connor, B. J., Boesch, H., Toon, G., Sen, B., Miller, C., and Crisp, D.: Orbiting Carbon Observatory: Inverse method and prospective error analysis, *J. Geophys. Res.*, 113, D05305, doi:10.1029/2006JD008336, 2008.](#)
- Dave, J. V.: Multiple scattering in a non-homogeneous, Rayleigh atmosphere, *J. Atmos. Sci.*, 22, 273–279, 1965.
- 1030 Dobber, M., Dirksen, R., Levelt, P., Van den Oord, G. H. J., Voors, R., Kleipool, Q., Jaross, G., Kowalewski, M., Hilsenrath, E., Leppelmeier, G., de Vries, J., Dierssen, W., and Rozemeijer, N.: Ozone monitoring instrument calibration, *IEEE T. Geosci. Remote*, 44, 1209–1238, doi:10.1109/TGRS.2006.869987, 2006.
- Douglass, A. R., Stolarski, R. S., Strahan, S. E., and Connell, P. S.: Radicals and reservoirs in the GMI chemistry and transport model: comparison to measurements, *J. Geophys. Res.*, 109, D16302, doi:10.1029/2004JD004632, 2004.
- 1035 Driscoll, C. T., Lawrence, G. B., Bulger, A. J., Butler, T. J., Cronan, C. S., Eagar, C., Lambert, K. F., Likens, G. E., Stoddard, J. L., and Weathers, K.: Acidic deposition in the northeastern United States: sources and inputs, ecosystem effects, and management strategies, *Bioscience*, 51, 180–198, doi:10.1641/0006-3568(2001)051[0180:ADITNU]2.0.CO;2, 2001.
- 1040 Du, Y.: New consolidation of emission and processing for air quality modeling assessment in Asia, Master’s thesis, University of Tennessee, available at: http://trace.tennessee.edu/utk_gradthes/372 (last access: August 2014), 2008.
- Duncan, B. N., Strahan, S. E., Yoshida, Y., Steenrod, S. D., and Livesey, N.: Model study of the cross-tropopause transport of biomass burning pollution, *Atmos. Chem. Phys.*, 7, 3713–3736, doi:10.5194/acp-7-3713-2007, 1045 2007.
- Eskes, H. J. and Boersma, K. F.: Averaging kernels for DOAS total-column satellite retrievals, *Atmos. Chem. Phys.*, 3, 1285–1291, doi:10.5194/acp-3-1285-2003, 2003.
- Guangdong Provincial Environmental Protection Monitoring Centre (GDEMC) and Environmental Protection Department, HKSAR (HKEPD): Pearl River Delta Regional Air Quality Monitoring Network – a report of monitoring results in 2006 (PRDAIR-2006-2), available at: [http://www.epd.gov.hk/epd/english/resources_](http://www.epd.gov.hk/epd/english/resources_pub/publications/m_report.html) 1050 [pub/publications/m_report.html](http://www.epd.gov.hk/epd/english/resources_pub/publications/m_report.html) (last access: April 2014), 2006.
- [Gu, D., Wang, Y., Smeltzer, C. and Boersma, K. F.: Anthropogenic emissions of NO_x over China: Reconciling the difference of inverse modeling results using GOME-2 and OMI measurements, *J. Geophys. Res.*, 119, 2169–8996, doi:10.1002/2014JD021644, 2014.](#)
- 1055 Guenther, A., Hewitt, C. N., Erickson, D., Fall, R., Geron, C., Graedel, T., Harley, P., Klinger, L., Lerdau, M., McKay, W. A., Pierce, T., Scholes, B., Steinbrecher, R., Tallamraju, R., Taylor, J., and Zimmerman, P.: A global model of natural volatile organic compound emissions, *J. Geophys. Res.*, 100, 8873–8892, doi:10.1029/94JD02950, 1995.
- Haagen-Smit, A. J.: Chemistry and physiology of Los Angeles smog, *Ind. Eng. Chem.*, 44, 1342–1346, 1952.

- 1060 Han, K. M., Lee, C. K., Lee, J., Kim, J., and Song, C. H.: A comparison study between model-predicted and OMI-retrieved tropospheric NO₂ columns over the Korean peninsula, *Atmos. Environ.*, 45, 2962–2971, doi:10.1016/j.atmosenv.2010.10.016, 2011.
- [Han, K. M., Lee, S., Chang, L. S., and Song, C. H.: A comparison study between CMAQ-simulated and OMI-retrieved NO₂ columns over East Asia for evaluation of NO_x emission fluxes of INTEX-B, CAPSS, and REAS inventories, *Atmos. Chem. Phys.*, 15, 1913–1938, doi:10.5194/acp-15-1913-2015, 2015.](#)
- 1065 He, Q., Li, C., Mao, J., Lau, A. K.-H., and Chu, D. A.: Analysis of aerosol vertical distribution and variability in Hong Kong, *J. Geophys. Res.*, 113, D14211, doi:10.1029/2008JD009778, 2008.
- [Herman, J. R., Celarier, E., and Larko, D.: UV 380 nm reflectivity of the Earth's surface, clouds and aerosols, *J. Geophys. Res.*, 106, 5335–5351, doi:10.1029/2000JD900584, 2001.](#)
- 1070 Herron-Thorpe, F. L., Lamb, B. K., Mount, G. H., and Vaughan, J. K.: Evaluation of a regional air quality forecast model for tropospheric NO₂ columns using the OMI/Aura satellite tropospheric NO₂ product, *Atmos. Chem. Phys.*, 10, 8839–8854, doi:10.5194/acp-10-8839-2010, 2010.
- Hess, M., Koepke, P., and Schult, I.: Optical properties of aerosols and clouds: the software package OPAC, *B. Am. Meteorol. Soc.*, 79, 831–844, 1998.
- 1075 [Huijnen, V., Eskes, H. J., Poupkou, A., Elbern, H., Boersma, K. F., Foret, G., Sofiev, M., Valdebenito, A., Flemming, J., Stein, O., Gross, A., Robertson, L., D'Isidoro, M., Kioutsioukis, I., Friese, E., Amstrup, B., Bergstrom, R., Strunk, A., Virra, J., Zyryanov, D., Maurizi, A., Melas, D., Peuch, V.-H., and Zerefos, C.: Comparison of OMI NO₂ tropospheric columns with an ensemble of global and European regional air quality models, *Atmos. Chem. Phys.*, 10, 3273–3296, doi:10.5194/acp-10-3273-2010, 2010.](#)
- 1080 Kleipool, Q. L., Dobber, M. R., de Haan, J. F., and Levelt, P. F.: Earth surface reflectance climatology from 3 years of OMI data, *J. Geophys. Res.*, 113, D18308, doi:10.1029/2008JD010290, 2008.
- Knutsson, H. and Westin, C.-F.: Normalized and differential convolution: methods for interpolation and filtering of incomplete and uncertain data, in: *Proceedings of Computer Vision and Pattern Recognition ('93)*, New York City, USA, 16–19 June 1993, 515–523, 1993.
- 1085 Kuhlmann, G., Hartl, A., Cheung, H. M., Lam, Y. F., and Wenig, M. O.: A novel gridding algorithm to create regional trace gas maps from satellite observations, *Atmos. Meas. Tech.*, 7, 451–467, doi:10.5194/amt-7-451-2014, 2014.
- Kurosu, T. P. and Celarier, E. A.: OMIPIXCOR Readme File, available at: http://disc.sci.gsfc.nasa.gov/Aura/data-holdings/OMI/documents/v003/OMPIXCOR_README_V003.pdf (last access: August 2014), 2010.
- 1090 [Lamsal, L. N., Martin, R. V., van Donkelaar, A., Steinbacher, M., Celarier, E. A., Bucsela, E., Dunlea, E. J., Pinto, J. P.: Ground-level nitrogen dioxide concentrations inferred from the satellite-borne Ozone Monitoring Instrument, *J. Geophys. Res.*, 113, D16, doi:10.1029/2007JD009235, 2008.](#)
- [Leitão, J., Richter, A., Vrekoussis, M., Kokhanovsky, A., Zhang, Q. J., Beekmann, M., and Burrows, J. P.: On the improvement of NO₂ satellite retrievals – aerosol impact on the airmass factors, *Atmos. Meas. Tech.*, 3, 475–493, doi:10.5194/amt-3-475-2010, 2010.](#)
- 1095 Levelt, P., van den Oord, G., Dobber, M., Malkki, A., Visser, H., de Vries, J., Stammes, P., Lundell, J., and Saari, H.: The ozone monitoring instrument, *IEEE T. Geosci. Remote*, 44, 1093–1101, doi:10.1109/TGRS.2006.872333, 2006.

- Lin, J.-T., Martin, R. V., Boersma, K. F., Sneep, M., Stammes, P., Spurr, R., Wang, P., Van Roozendael, M.,
1100 Clémer, K., and Irie, H.: Retrieving tropospheric nitrogen dioxide from the Ozone Monitoring Instrument:
effects of aerosols, surface reflectance anisotropy, and vertical profile of nitrogen dioxide, *Atmos. Chem.
Phys.*, 14, 1441–1461, doi:10.5194/acp-14-1441-2014, 2014.
- Lucht, W., Schaaf, C., and Strahler, A.: An algorithm for the retrieval of albedo from space using semiempirical
BRDF models, *IEEE T. Geosci. Remote*, 38, 977–998, doi:10.1109/36.841980, 2000.
- 1105 Malm, W., Gebhart, K., Molenaar, J., Cahill, T., Eldred, R., and Huffman, D.: Examining the relationship between
atmospheric aerosols and light extinction at Mount Rainier and North Cascades National Parks, *Atmos.
Environ.*, 28, 347–360, doi:10.1016/1352-2310(94)90110-4, 1994.
- [McLinden, C. A., Fioletov, V., Boersma, K. F., Kharol, S. K., Krotkov, N., Lamsal, L., Makar, P. A., Martin,
R. V., Veefkind, J. P., and Yang, K.: Improved satellite retrievals of NO₂ and SO₂ over the Canadian oil
1110 sands and comparisons with surface measurements, *Atmos. Chem. Phys.*, 14, 3637–3656, doi:10.5194/acp-
14-3637-2014, 2014.](#)
- [Mijling, B. and van der A, R. J. and Zhang, Q.: Regional nitrogen oxides emission trends in East Asia observed
from space, *Atmos. Chem. Phys.*, 13, 12003–12012, doi:10.5194/acp-13-12003-2013, 2013.](#)
- [Mueller, M., Wagner, M., Barmpadimos, I., and Hueglin, C.: Two-week NO₂ maps for the City of Zurich,
1115 Switzerland, derived by statistical modelling utilizing data from a routine passive diffusion sampler network,
Atmos. Environ., 106, 1 – 10, doi:10.1016/j.atmosenv.2015.01.049, 2015.](#)
- National Centers for Environmental Prediction/National Weather Service/NOAA/U.S. Department of Com-
merce: NCEP FNL operational model global tropospheric analyses, April 1997 to June 2007, available at:
http://rda.ucar.edu/datasets/ds083.0/ (last access: December 2013), 1997.
- 1120 Palmer, P. I., Jacob, D. J., Chance, K., Martin, R. V., Robert, J. D., Kurosu, T. P., Bey, I., Yantosca, R., Fiore, A.,
and Li, Q.: Air mass factor formulation for spectroscopic measurements from satellites: application to
formaldehyde retrievals from the global ozone monitoring experiment, *J. Geophys. Res.*, 106, 14539–14550,
doi:10.1029/2000JD900772, 2001.
- Platt, U. and Stutz, J.: *Differential Optical Absorption Spectroscopy: Principles and Applications*, Springer
1125 Verlag, Berlin Heidelberg, 2008.
- Pleim, J. E. and Chang, J. S.: A non-local closure model for vertical mixing in the convective boundary layer,
Atmos. Environ., 26, 965–981, doi:10.1016/0960-1686(92)90028-J, 1992.
- Rozanov, A., Rozanov, V., Buchwitz, M., Kokhanovsky, A., and Burrows, J.: SCIATRAN 2.0 – a new radiative
transfer model for geophysical applications in the 175–2400 nm spectral region, *Adv. Space Res.*, 36, 1015–
1130 1019, 2005.
- Rozanov, V., Kurosu, T., and Burrows, J.: Retrieval of atmospheric constituents in the uv-visible: a new
quasi-analytical approach for the calculation of weighting functions, *J. Quant. Spectrosc. Ra.*, 60, 277–299,
doi:10.1016/S0022-4073(97)00150-7, 1998.
- Rozanov, V. V. and Rozanov, A. V.: Differential optical absorption spectroscopy (DOAS) and air mass factor
1135 concept for a multiply scattering vertically inhomogeneous medium: theoretical consideration, *Atmos. Meas.
Tech.*, 3, 751–780, doi:10.5194/amt-3-751-2010, 2010.

- Russell, A. R., Perring, A. E., Valin, L. C., Bucsel, E. J., Browne, E. C., Wooldridge, P. J., and Cohen, R. C.: A high spatial resolution retrieval of NO₂ column densities from OMI: method and evaluation, *Atmos. Chem. Phys.*, 11, 8543–8554, doi:10.5194/acp-11-8543-2011, 2011.
- 1140 [Schaub, D., Boersma, K. F., Kaiser, J. W., Weiss, A. K., Folini, D., Eskes, H. J., and Buchmann, B.: Comparison of GOME tropospheric NO₂ columns with NO₂ profiles deduced from ground-based in situ measurements, *Atmos. Chem. Phys.*, 6, 3211–3229, doi:10.5194/acp-6-3211-2006, 2006.](#)
- Skamarock, W. C., Klemp, J. B., Dudhia, J., Gill, D. O., Barker, D. M., Duda, M. G., Huang, X.-Y., Wang, W., and Powers, J. G.: A description of the advanced research WRF Version 3, National Center for Atmospheric Research, Boulder, Colorado, USA, NCAR/TN-475+STR, doi:10.5065/D68S4MVH, 2008.
- 1145 Solomon, S., Schmeltekopf, A., and Sanders, R.: On the interpretation of zenith sky absorption measurements, *J. Geophys. Res.*, 92, 8311–8319, doi:10.1029/JD092iD07p08311, 1987.
- Strahan, S. E., Duncan, B. N., and Hoor, P.: Observationally derived transport diagnostics for the lowermost stratosphere and their application to the GMI chemistry and transport model, *Atmos. Chem. Phys.*, 7, 2435–2445, doi:10.5194/acp-7-2435-2007, 2007.
- 1150 Streets, D. G., Bond, T. C., Carmichael, G. R., Fernandes, S. D., Fu, Q., He, D., Klimont, Z., Nelson, S. M., Tsai, N. Y., Wang, M. Q., Woo, J.-H., and Yarber, K. F.: An inventory of gaseous and primary aerosol emissions in Asia in the year 2000, *J. Geophys. Res.*, 108, 8809, doi:10.1029/2002JD003093, 2003.
- [Tang, W., Cohan, D. S., Morris, G. A., Byun, D. W., and Luke, W. T.: Influence of vertical mixing uncertainties on ozone simulation in {CMAQ}, *Atmos. Environ.*, 45, 2898 – 2909, doi:http://dx.doi.org/10.1016/j.atmosenv.2011.01.057, 2011.](#)
- 1155 Wanner, W., Strahler, A. H., Hu, B., Lewis, P., Muller, J.-P., Li, X., Schaaf, C. L. B., and Barnsley, M. J.: Global retrieval of bidirectional reflectance and albedo over land from EOS MODIS and MISR data: theory and algorithm, *J. Geophys. Res.*, 102, 17143–17161, doi:10.1029/96JD03295, 1997.
- 1160 Willmott, C. J.: On the validation of models, *Phys. Geogr.*, 2, 184–194, <http://www.tandfonline.com/doi/abs/10.1080/02723646.1981.10642213>, 1981.
- World Meteorological Organization: WMO Guide to Meteorological Instruments and Methods of Observation, World Meteorological Organization, 7th edn., Geneva, 2008.
- Wu, Q., Wang, Z., Chen, H., Zhou, W., and Wenig, M.: An evaluation of air quality modeling over the Pearl River Delta during November 2006, *Meteorol. Atmos. Phys.*, 116, 113–132, doi:10.1007/s00703-011-0179-z, 2012.
- 1165 [Xie, B., Fung, J. C. H., Chan, A., and Lau, A.: Evaluation of nonlocal and local planetary boundary layer schemes in the WRF model, *J. Geophys. Res.*, 117, doi:10.1029/2011JD017080, 2012.](#)
- Yamartino, R. J.: Nonnegative, conserved scalar transport using grid-cell-centered, spectrally constrained Blackman cubics for applications on a variable-thickness mesh, *Mon. Weather Rev.*, 121, 753–763, doi:10.1175/1520-0493(1993)121<0753:NCSTUG>2.0.CO;2, 1993.
- 1170 Yarwood, G., Rao, S., Yocke, M., and Whitten, G. Z.: Updates to the Carbon Bond chemical mechanism: CB05. Final Report to the U.S. EPA, RT-0400675, available at: http://www.camx.com/publ/pdfs/cb05_final_report_120805.pdf (last access: February 2014), 2005.

- 1175 Zhang, Q., Streets, D. G., Carmichael, G. R., He, K. B., Huo, H., Kannari, A., Klimont, Z., Park, I. S., Reddy, S.,
Fu, J. S., Chen, D., Duan, L., Lei, Y., Wang, L. T., and Yao, Z. L.: Asian emissions in 2006 for the NASA
INTEX-B mission, *Atmos. Chem. Phys.*, 9, 5131–5153, doi:10.5194/acp-9-5131-2009, 2009.
- Zhang, R., Bian, Q., Fung, J. C., and Lau, A. K.: Mathematical modeling of seasonal variations
in visibility in Hong Kong and the Pearl River Delta region, *Atmos. Environ.*, 77, 803–816,
1180 doi:10.1016/j.atmosenv.2013.05.048, 2013.
- Zhou, Y., Brunner, D., Boersma, K. F., Dirksen, R., and Wang, P.: An improved tropospheric NO₂ retrieval for
OMI observations in the vicinity of mountainous terrain, *Atmos. Meas. Tech.*, 2, 401–416, doi:10.5194/amt-
2-401-2009, 2009.
- Zhou, Y., Brunner, D., Spurr, R. J. D., Boersma, K. F., Sneep, M., Popp, C., and Buchmann, B.: Accounting for
1185 surface reflectance anisotropy in satellite retrievals of tropospheric NO₂, *Atmos. Meas. Tech.*, 3, 1185–1203,
doi:10.5194/amt-3-1185-2010, 2010.
- Zyrichidou, I., Koukouli, M. E., Balis, D. S., Kioutsioukis, I., Poupkou, A., Katragkou, E., Melas, D.,
Boersma, K., and van Roozendaal, M.: Evaluation of high resolution simulated and OMI re-
trieved tropospheric NO₂ column densities over Southeastern Europe, *Atmos. Res.*, 122, 55–66,
1190 doi:10.1016/j.atmosres.2012.10.028, 2013.

~~Ancillary parameters used for deriving tropospheric column densities from OMI.~~

Table 1. Standard set of ancillary parameters used in the AMF sensitivity study.

| Ancillary Parameter | Value |
|--------------------------------------|----------------------------|
| solar zenith angle (SZA) | 48° |
| viewing zenith angle (VZA) | 0° (nadir) |
| relative azimuth angle (RAA) | 180° |
| terrain height | 0.0 km |
| surface reflectance | 0.05 |
| aerosol/cloud radiance fraction | 0.00 |
| temperature and pressure profiles | WRF average |
| NO ₂ and aerosol profiles | CMAQ averages (see Fig. 2) |

Table 2. Error measures used to compare observations and model. $\langle \cdot \rangle$ is the mean value and σ_x and σ_y are standard deviations.

| | |
|---|--|
| <u>Index of agreement (Willmott, 1981)</u> | $IOA = 1 - \frac{\sum_{i=1}^N (x_i - y_i)^2}{\sum_{i=1}^N (x_i - \langle y \rangle + y_i - \langle y \rangle)^2}$ |
| <u>Pearson's correlation coefficient</u> | $r = \frac{1}{N-1} \sum_{i=1}^N \left(\frac{y_i - \langle y \rangle}{\sigma_y} \right) \left(\frac{x_i - \langle x \rangle}{\sigma_x} \right)$ |
| <u>Root mean square error</u> | $RMSE = \sqrt{\frac{1}{N} \sum_{i=1}^N (x_i - y_i)^2}$ |
| <u>Coefficient of variation of the RMSE</u> | $CV = \frac{RMSE}{\langle y \rangle}$ |
| <u>Mean bias</u> | $MB = \frac{1}{N} \sum_{i=1}^N (x_i - y_i)$ |
| <u>Normalised mean bias</u> | $NMB = \frac{MB}{\langle y \rangle}$ |

~~Sensitivity of AMF to a change of 0.01 in surface reflectance for different surface reflectance. The lines show the sensitivity for a polluted and clean aerosol profile (Fig. 2).~~

~~Scatter plot between CMAQ and PRD-4 at (a) GZFS and (b) HKSZ.~~

Table 3. Difference between OMI NO₂ datasets (level 2) due to different ancillary parameters.

| <u>Dataset</u> | <u>Compared to</u> | <u>All VCDs</u> | | <u>10% highest VCDs</u> | | <u>Different ancillary parameter</u> |
|-----------------|--------------------|------------------------|-----------------------|-------------------------|-----------------------|--|
| | | <u>NMB^a</u> | <u>CV^a</u> | <u>NMB^a</u> | <u>CV^a</u> | |
| <u>OMNO2-SW</u> | <u>OMNO2-SP</u> | <u>+11.4</u> | <u>13.4</u> | <u>+13.2</u> | <u>14.3</u> | <u>a-priori NO₂ profile</u> |
| <u>HKOMI-1</u> | <u>OMNO2-SW</u> | <u>+11.0</u> | <u>20.9</u> | <u>+11.3</u> | <u>19.4</u> | <u>surface reflectance^b</u> |
| <u>HKOMI-2</u> | <u>HKOMI-1</u> | <u>+24.1</u> | <u>24.1</u> | <u>+29.9</u> | <u>29.9</u> | <u>aerosols (case 2)</u> |
| <u>HKOMI-3</u> | <u>HKOMI-1</u> | <u>+8.1</u> | <u>9.3</u> | <u>+12.2</u> | <u>12.5</u> | <u>aerosols (case 3)</u> |
| <u>HKOMI-4</u> | <u>HKOMI-1</u> | <u>+6.0</u> | <u>8.4</u> | <u>+9.8</u> | <u>11.2</u> | <u>aerosols (case 4)</u> |
| <u>HKOMI-4</u> | <u>OMNO2-SP</u> | <u>+31.0</u> | <u>34.0</u> | <u>+38.3</u> | <u>40.0</u> | <u>all</u> |

^a in percent, ^b difference are also due to other difference between the OMNO2 and HKOMI retrieval, e.g. temperature profiles.

Table 4. The AMFs for different aerosol treatment cases for the standard parameters and profiles (Fig. 2).

| <u>Aerosol parametrisation</u> | <u>PRD-1 Case 1</u> | <u>Case 2</u> | | <u>Cases 3 & 4</u> | |
|------------------------------------|---------------------|---------------|-----------------|------------------------|-----------------|
| | | <u>clean</u> | <u>polluted</u> | <u>clean</u> | <u>polluted</u> |
| <u>NO₂ clean</u> | <u>0.84</u> | <u>0.68</u> | <u>0.39</u> | <u>0.77</u> | <u>0.74</u> |
| <u>NO₂ polluted</u> | <u>0.82</u> | <u>0.65</u> | <u>0.35</u> | <u>0.74</u> | <u>0.70</u> |

Table 5. The difference between raw and processed CMAQ data due to the spatial resolution of the satellite instrument (area averaging error).

| | <u>IOA</u> | <u>r</u> | <u>MB^a</u> | <u>NMB^b</u> | <u>RMSE^a</u> | <u>CV^b</u> |
|---------------------|-------------|--------------|-----------------------|------------------------|-------------------------|-----------------------|
| <u>HK & SZ</u> | <u>0.54</u> | <u>+0.25</u> | <u>-4.6</u> | <u>-16</u> | <u>17.6</u> | <u>59</u> |
| <u>FS & GZ</u> | <u>0.77</u> | <u>+0.67</u> | <u>-1.6</u> | <u>-12</u> | <u>7.0</u> | <u>52</u> |
| <u>all stations</u> | <u>0.69</u> | <u>+0.56</u> | <u>-2.9</u> | <u>-17</u> | <u>9.3</u> | <u>54</u> |

^a in ppbv, ^b in percent.

Table 6. OMI evaluation with the RAQM network.

| <u>Case-Dataset</u> | IOA | r | MB ^a | NMB ^b | RMSE ^a | CV ^b |
|---------------------------|-------------|--------------|-----------------|------------------|-------------------|-----------------|
| Hong Kong and Shenzhen | | | | | | |
| SP2-OMNO2-SP | 0.31 | +0.19 | -17.5 | -54 | 23.4 | 73 |
| PRD-1-OMNO2-SW | <u>0.34</u> | <u>+0.10</u> | <u>-13.0</u> | <u>-40</u> | <u>21.6</u> | <u>67</u> |
| HKOMI-1 | 0.43 | +0.24 | -8.8 | -27 | 20.6 | 64 |
| PRD-2-HKOMI-2 | 0.52 | +0.25 | -0.7 | -2 | 21.9 | 68 |
| PRD-3-HKOMI-3 | 0.44 | +0.20 | -6.3 | -20 | 20.7 | 64 |
| PRD-4-HKOMI-4 | 0.45 | +0.24 | -7.4 | -23 | 20.1 | 62 |
| Foshan and Guangzhou | | | | | | |
| SP2-OMNO2-SP | 0.43 | +0.47 | -14.3 | -48 | 20.9 | 71 |
| PRD-1-OMNO2-SW | <u>0.46</u> | <u>+0.45</u> | <u>-13.1</u> | <u>-44</u> | <u>20.2</u> | <u>68</u> |
| HKOMI-1 | 0.48 | +0.41 | -10.7 | -36 | 19.2 | 65 |
| PRD-2-HKOMI-2 | 0.58 | +0.42 | -5.2 | -18 | 17.8 | 60 |
| PRD-3-HKOMI-3 | 0.50 | +0.40 | -8.5 | -29 | 18.4 | 62 |
| PRD-4-HKOMI-4 | 0.53 | +0.46 | -8.7 | -29 | 17.9 | 60 |
| All stations | | | | | | |
| SP2-OMNO2-SP | 0.40 | +0.35 | -10.7 | -41 | 18.7 | 73 |
| PRD-1-OMNO2-SW | <u>0.42</u> | <u>+0.29</u> | <u>-8.2</u> | <u>-32</u> | <u>18.2</u> | <u>71</u> |
| HKOMI-1 | 0.46 | +0.31 | -5.6 | -22 | 18.2 | 71 |
| PRD-2-HKOMI-2 | 0.53 | +0.32 | +0.7 | +3 | 19.6 | 76 |
| PRD-3-HKOMI-3 | 0.47 | +0.29 | -3.3 | -13 | 18.6 | 72 |
| PRD-4-HKOMI-4 | 0.50 | +0.35 | -3.9 | -15 | 17.6 | 68 |

^a in ppbv, ^b in percent.

Table 7. NO₂ mean values (in ppbv) at the RAQM network stations for CMAQ, network and OMI datasets.

| Stations | CMAQ (raw) | CMAQ (processed) | RAQM | SP2-OMNO2-SP | PRD-1-OMNO2-SW | PRD-2-HKOMI-1 | PRD-3-HKOMI-2 | PRD-4-HKOMI-3 |
|----------------------|---------------|---------------------|------|-------------------------|---------------------------|--------------------------|--------------------------|--------------------------|
| HKSZ-HKSZ | 29.3 | 25.1 | 32.9 | 14.9 | <u>19.3</u> | 23.4 | 31.6 | 25.9 |
| FSGZ-FSGZ | 13.7 | 12.0 | 29.5 | 15.2 | <u>16.5</u> | 18.9 | 24.4 | 21.0 |
| All stations | 18.6 | 15.7 | 25.3 | 14.5 | <u>16.9</u> | 19.4 | 25.6 | 21.6 |

Table 8. Evaluation of the time series of CMAQ with OMI NO₂ VCDs in the two areas marked in Fig. 4.

| Dataset | OMI Mean ^a | IOA | <i>r</i> | MB ^a | NMB ^b |
|-------------------------------|-----------------------|-------------|-------------|-----------------|------------------|
| Foshan and Guangzhou (area) | | | | | |
| SP2-OMNO2-SP | 2.5 | 0.57 | 0.37 | -0.5 | -18 |
| PRD-1-OMNO2-SW | <u>2.8</u> | <u>0.57</u> | <u>0.39</u> | <u>-0.7</u> | <u>-26</u> |
| HKOMI-1 | 3.1 | 0.55 | 0.35 | -1.1 | -35 |
| PRD-2-HKOMI-2 | 4.0 | 0.51 | 0.35 | -2.0 | -49 |
| PRD-3-HKOMI-3 | 3.5 | 0.56 | 0.43 | -1.5 | -42 |
| PRD-4-HKOMI-4 | 3.4 | 0.54 | 0.37 | -1.3 | -40 |
| Hong Kong and Shenzhen (area) | | | | | |
| SP2-OMNO2-SP | 1.7 | 0.51 | 0.57 | +1.2 | +73 |
| PRD-1-OMNO2-SW | <u>2.2</u> | <u>0.64</u> | <u>0.59</u> | <u>+0.8</u> | <u>+37</u> |
| HKOMI-1 | 2.4 | 0.65 | 0.51 | +0.6 | +24 |
| PRD-2-HKOMI-2 | 3.2 | 0.66 | 0.45 | -0.2 | -8 |
| PRD-3-HKOMI-3 | 2.7 | 0.75 | 0.58 | +0.2 | +9 |
| PRD-4-HKOMI-4 | 2.6 | 0.71 | 0.56 | +0.4 | +15 |

^a in 10¹⁶ molecules cm⁻², ^b in percent.

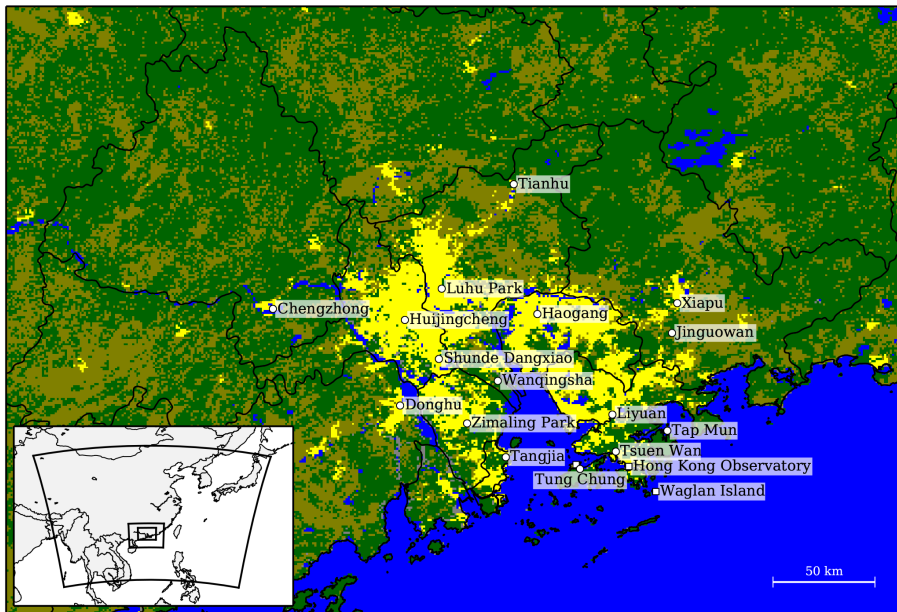


Figure 1. The large figure shows the CMAQ model domain (D3) with MODIS land categories in the Pearl River Delta (PRD) region grouped into the following categories: forest (darkgreen), crop lands (olive), bare land (grey), urban areas (yellow) and water (blue). The stations of the PRD Regional Air Quality Monitoring (RAQM) network and HKO automatic weather stations are marked by circles and squares, respectively. The small figure shows the three CMAQ model domains which are D1, D2 and D3 from the largest to smallest.

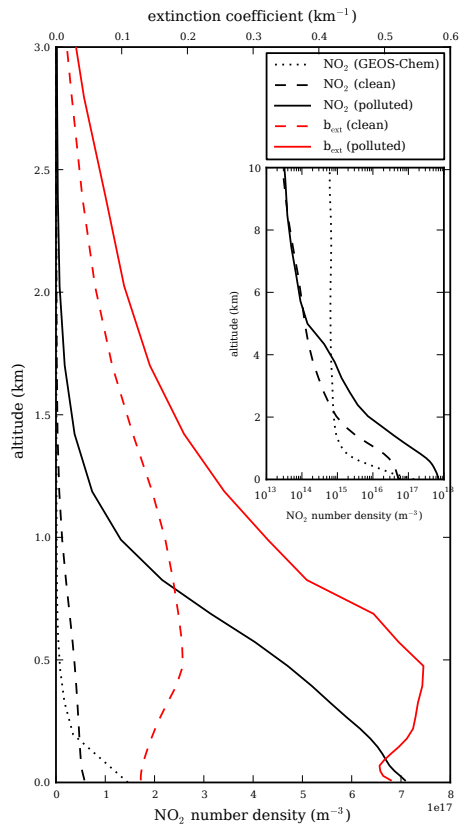


Figure 2. Averaged CMAQ NO_2 and b_{ext} profiles under “clean” and “polluted” conditions. A NO_2 profiles was categorised as polluted, if the ground number density was larger than $4.8 \times 10^{17} \text{ m}^{-3}$ (about 20 ppbv). A b_{ext} profile was categorised as polluted, if the ground extinction coefficient was larger than 0.4. The clean b_{ext} profile has an AOT of 0.3 while the polluted as an AOT of 0.6. In addition, an annual GEOS-Chem NO_2 profile is shown for Hong Kong ($2^\circ \times 2.5^\circ$ spatial resolution).

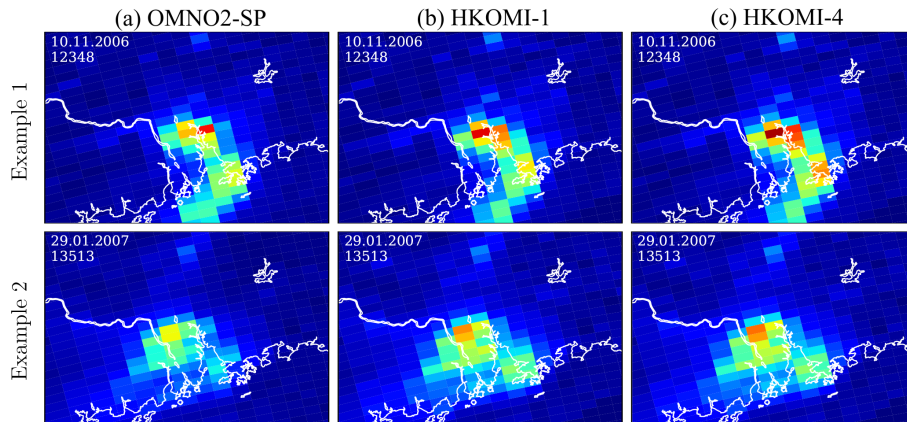


Figure 3. Two example orbits of OMI NO₂ distributions for SP2OMNO2-SP, PRD-1HKOMI-1 and PRD-4HKOMI-4. The overall spatial distribution is similar but different in details. The PRD-1HKOMI-1 and PRD-4HKOMI-4 datasets have larger NO₂ column densities than the standard product (SP2)OMNO2-SP.

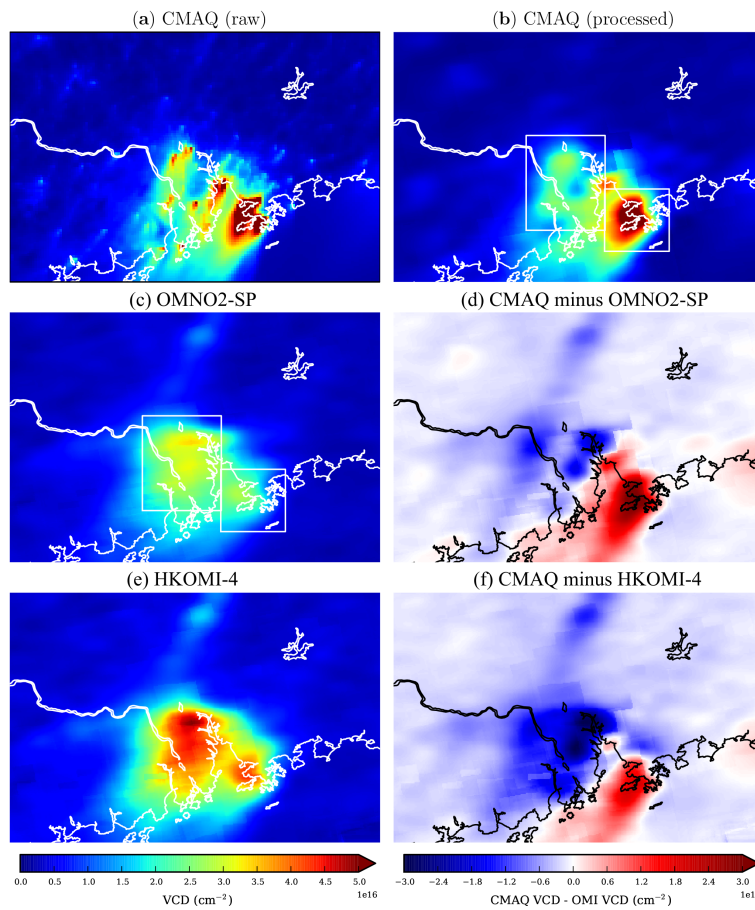


Figure 4. Four-month mean distribution of (a) raw and (b) processed CMAQ NO₂ VCDs, (c) OMI-SP2 OMNO2-SP VCDs and (d) the difference to CMAQ, (e) OMI-PRD-4HKOMI-4 VCDs and (f) the difference to CMAQ.

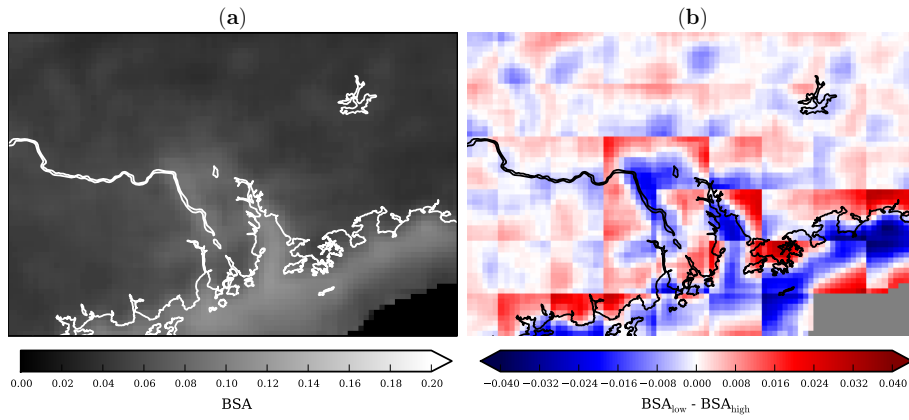


Figure 5. (a) The averaged MODIS black-sky albedo (BSA) and (b) the differences between low- and high-resolution BSAs.

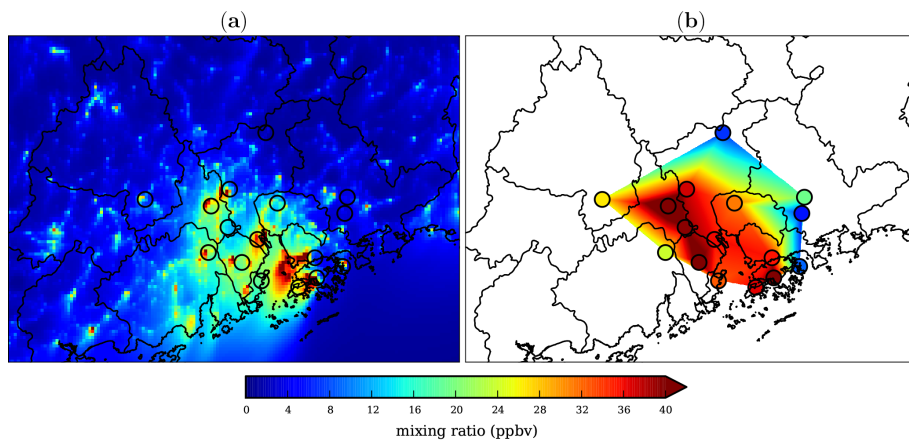


Figure 6. Ground level NO₂ mixing ratios averaged for October 2006 to January 2007: (a) CMAQ simulation and (b) RAQM network measurements. The values between stations have been estimated by linear interpolation.

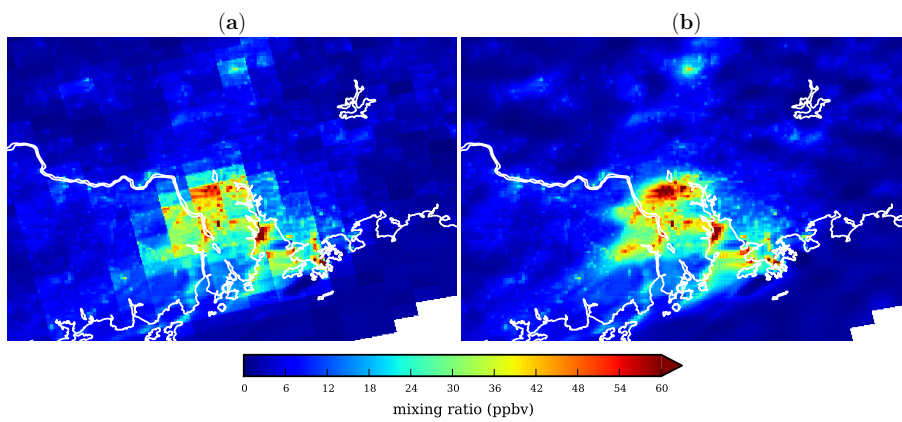


Figure 7. OMI ground mixing ratios from orbit number 13513 on 29 January 2007 comparing a (a) “standard” and (b) newly developed gridding algorithm (Kuhlmann et al., 2014). The discontinuous map created by the “standard” algorithm is difficult to interpret while the new algorithms makes an analysis of the spatial distribution easier.